npj | computational materials

Article

Published in partnership with the Shanghai Institute of Ceramics of the Chinese Academy of Sciences

https://doi.org/10.1038/s41524-025-01783-3

Unified generalized universal equation of states for magnetic Co, Cr, Fe, Mn and Ni: an approach for non-collinear atomistic modelling

Isaac Toda-Caraballo [1] ✉, Jan S. Wróbel [2] & Duc Nguyen-Manh [3,4]

Despite great efforts to study magnetic properties of 3d-transition metals from both fundamental and applied interest, there exists no modelling approach that would be able to describe magnetic and structural phase stability of all these elements on a unified formalism. In this work, we propose a qualitative improvement of the Generalisation of the Universal Equation of States (GUES) that we presented recently in a previous work developed and tested for cubic structures in Fe. The GUES is now extended to other 3d-transition magnetic elements and crystal lattices, where now magnetic Co, Cr, Mn, and Ni are considered, including both cubic and hexagonal structures, and also covering ferromagnetic (FM) and antiferromagnetic (AFM) configurations. An extensive database has been developed and used to fit all parameters and functions for all considered elements. The current GUES unifies the two previous separate approaches for FM and AFM configurations, allowing for non-collinear calculations, which are tested for Co, Cr, Fe, Mn and Ni. The approach is consistent with the Stoner model of band magnetism and the Ginzburg-Landau approximation used in the magnetic cluster expansion method, as well as with non-collinear magnetism described in the Heisenberg-Landau Hamiltonians. Importantly, it also includes magneto-volume effects, which are important for understanding defect properties in magnetic materials. This work permits considering the development of a new class of magnetic interatomic potentials for non-collinear simulations based on the approach proposed by the GUES. (The figures shown in this article can be seen in colour only in the electronic version).

The presence of magnetism has a strong implication for structural stability in a large variety of materials such as single-element magnetic transition metals, steels and numerous other classes of functional materials and high-entropy alloys for nuclear energy applications. Despite the crucial role of magnetism in the aforementioned materials, modeling efforts to provide a quantitative theory of the interplaying between magnetic and structural properties have been notably lacking. In a pioneering work by Hasegawa and Pettifor[1], the authors showed that the presence of magnetism stabilizes the bcc phase of iron. A theoretical treatment of itinerant electron magnetism that highlighted the importance of quantum mechanical description of spin associated with electronic band structure from density functional theory (DFT) calculations has been reviewed by Kubler[2] within Stoner formalism[3]. Using DFT calculations, the magnetic cluster expansion method has been developed to parametrize the adiabatic magnetic energy and investigate complex multi-interactions from electron spins[4,5] as well as structural phase transition between BCC (Body Centered Cubic) and FCC (Face Centered Cubic) phases of Fe[6]. A constrained non-collinear magnetism approach developed within DFT formulation has been employed by Nguyen-Manh and co-workers to investigate the effect electron spin orientation on irradiated defect configurations and structural

[1]Materalia Group/Physical Metallurgy Department, National Center for Metallurgical Research (CENIM-CSIC), Madrid, Spain. [2]Faculty of Materials Science and Engineering, Warsaw University of Technology, Warsaw, Poland. [3]CCFE, United Kingdom Atomic Energy Authority, Abingdon, Oxfordshire, UK. [4]Department of Materials, University of Oxford, Oxford, UK. ✉e-mail: isaac.toda@cenim.csic.es

phase transition in Fe and Fe-Cr alloys[3,7,8]. A first ab-initio model considering the change in magnitude of magnetic moments in terms of temperature-induced longitudinal spin fluctuation for the exchange interaction parameters of the Hamiltonian for BCC-Fe and FCC-Ni has been proposed by Ruban et al.[9] and further investigated by Ma et al.[8,10]. A combined Landau model with Heisenberg Hamiltonian has also been used for magnetic cluster expansion spanning a broad range of alloy compositions, and a large variety of chemical and magnetic configurations has been developed for FCC Fe–Ni alloys[11]. Most recently, a great interest has been paid for developing magnetic machine learning potentials using spin-polarized ab-initio database[12–14] with Heisenberg Hamiltonian to model magnetic properties of Fe[15], extended deep learning DFT Hamiltonian for magnetic superstructures[16,17], and using the Materials Project database to study Mn-based stable magnetic materials[18]. Therefore, the key motivation of this paper is to propose a generalized formalism for investigating all important magnetic 3 d transition elements (Co, Cr, Fe, Mn, Ni) from the large constrained magnetic calculations DFT data base, and to propose an approach which could systematically study magnetic properties for such 3 d transition elements considering structural stability, non-collinear magnetism, longitudinal spin fluctuation and magneto-volume effects on equal footing.

In the scope of developing interatomic potentials for Molecular Dynamic (MD) simulations with magnetic contribution, a novel approach for magnetic interatomic potential for ferromagnetic Fe was proposed recently[19] which was tested on transformation paths, vacancies, stresses, A15 and C15 lattices, elastic properties, dumbbell configurations and γ-surfaces, as well as predicting correctly the volume-magnetic moment relationship, including low-spin configuration for low volumes and high-spin configuration for larger volumes in FCC, demonstrating the existence of such functions and their predictability. The formulation makes use of the Generalized Universal Equation of States (GUES), which is based on the Universal Equation of States (UES) proposed by Rosé and Vinet[20,21].

The approach follows a different viewpoint as compared to other attempts and formulations to simulate magnetism in molecular dynamics, since it does not follow the classical embedded atom method (EAM)[22,23] or some of their modifications via additional terms[24,25] in line with the Stoner model of band magnetism and the Ginzburg-Landau model. Neither the many-body force potentials[26,27] share the formulation with the GUES, although it has some similarities with the non-collinear magnetic many-body potentials based on the Heisenberg-Landau Hamiltonians[8] and the inter-site magnetic interaction parameters. Some works have used Machine Learning (ML) tools, showing the capability of this technique to incorporate collinear magnetic configurations for atomistic simulations[13,28], while others opted for adding some neural network correction terms to the EAM method[14]. More recently, non-collinear magnetic atomic cluster expansions were trained with collinear and non-collinear magnetic configurations for iron, showing good predictability and transferability[15].

As stated in our previous work[19], the original UES established that there a unique function E(*V*) that describes the evolution of the energy for all solids with respect to volume variations:

$$E(V) = E_g e^{-\frac{V-V_g}{K_g}}\left(1+\frac{V-V_g}{K_g}\right) \tag{1}$$

where E_g is the ground state energy, V_g is the volume at the ground state, and K_g the corresponding volume scaling function. Such a result has been extensively validated in the literature and widely applied to predict material properties related to volume[29–35]. Nevertheless, the UES is understood and generally applied for the ground state, as well as logically its experimental validation. The proposed GUES is more general and applies to any state, including different magnetic configurations. In other words, the results obtained in ref. 19 demonstrated, in the case Fe, that any crystal lattice in non-magnetic (NM) configuration as well as in ferromagnetic (FM) or antiferromagnetic (AFM) configurations, follows Eq. (1) if the crystal lattice and magnetic configuration are maintained. As an illustrative example, a deformed Body-centered cubic (BCC) lattice with dissimilar cell parameters $\langle a, b, c\rangle$ (not strictly BCC as it is not cubic anymore) and a constant magnetic moment M in ferromagnetic configuration, will follow Eq. (1) for volume variations (therefore, with constant $\langle b/a, c/a\rangle$ ratios) with certain E_g, V_g, and K_g values. Such E_g, V_g, and K_g values are not the global ground state, but they refer to metastable configurations (i.e. local ground states) of such lattice and magnetic configuration. That means that for such a BCC with constant $\langle b/a, c/a\rangle$ ratios and magnetic moment M in ferromagnetic configuration, E_g is its minimum energy, which occurs at the volume V_g. Again, such E_g and V_g are not the (global) ground state energy and ground state volume, but the local ones for such $\langle b/a, c/a\rangle$ structure.

The variables E_g, V_g, and K_g are therefore dependent on the magnetic moment, magnetic configuration, and the lattice. Nevertheless, in view of the development of an interatomic potential, a distance-dependent function ρ (scaled distance) was proposed in ref. 19 to substitute the "lattice" for "interatomic distances":

$$\rho_{ij} = \frac{r_{ij}^{\,3}}{V} \tag{2}$$

where r_{ij} is the distance between atoms i and j and V is the atomic volume of atom i according to the system volume. This variable ρ_{ij} describes then the set of distances of a certain lattice. Such a set of scaled distances between atoms is different from one lattice to another, but the same for a certain lattice under different volumes. Therefore, it can be used as a descriptive variable of different configurations.

Finally, in this work, the expression of the energy E of the system with N atoms as a function of volume $\boldsymbol{V}$ of such a system is expressed as:

$$E = \sum_{i=1}^{N} E_g^i(\boldsymbol{\rho},\boldsymbol{M})\, e^{-\frac{V-\sum_{i=1}^{N} V_g^i(\boldsymbol{\rho},\boldsymbol{M})}{\sum_{i=1}^{N} K_g^i(\boldsymbol{\rho},\boldsymbol{M})}}\left(1+\frac{\boldsymbol{V}-\sum_{i=1}^{N} V_g^i(\boldsymbol{\rho},\boldsymbol{M})}{\sum_{i=1}^{N} K_g^i(\boldsymbol{\rho},\boldsymbol{M})}\right) \tag{3}$$

where $\mathbf{V}$ is the volume of the system, the $\boldsymbol{\rho} = \langle \rho_{i1}, \rho_{i2}\rho_{i3}, \ldots, \rho_{iN}, \ldots\rangle$ and $\boldsymbol{M} = \langle \vec{M}_1, \vec{M}_2, \vec{M}_3, \ldots, \vec{M}_N, \ldots\rangle$, being ρ_{ij} the scaled distance between atom i and j (as defined in Eq. (2)) and $\vec{M}_j$ the magnetic moment of atom j, respectively. It is worth noting that the calculation of the energy E is now more general than in our previous publication[19], which was defined to provide the idea of the contribution to the energy of each individual atom, as it occurs on MD simulations for the EAM approach. In a certain system, these energy contributions were equal for an undistorted lattice under FM configuration, and therefore the energy was correctly computed for the analysed cases in ref. 19. Nevertheless, under the DFT approach, there is not a sum of energy-per-atom, but only the total energy of the system is calculated. Thus, in order to be more general in the current GUES, the equation of the energy of the system is now revised. Additionally, with this functional form, the energy dependence of the volume will always fulfill the UES as shown in Eq. (1) for any atomic arrangement, including those with atomic coordinates moving from ideal positions, as well as for different magnetic moments and spin orientations.

In our previously published paper[19], even though a magnetic interatomic potential for ferromagnetic configurations was developed, two main aspects of that approach needed to be revisited in order to obtain a robust approach for magnetism:

1. The GUES was proposed differently for ferromagnetic and antiferromagnetic. In other words, the functions describing E_g, V_g, and K_g were different for different magnetic configurations. In this work, we have unified the GUES, where the same formulation is applied for non-magnetic, ferromagnetic, and antiferromagnetic configurations, where the difference is the existence of different contributions in the same formulation, rather than different parameters. This opens the door to propose a formulation for non-collinear molecular dynamic simulations.

2. The GUES was proved only for Fe in cubic structures, and a more complete analysis in other elements needs to be carried out. In this case, in addition to completing Fe for the hexagonal lattices, we have selected Cr, Mn, Co and Ni (all for cubic and hexagonal lattices), which correspond to the previous and posterior atomic numbers in the periodic table, also with a variety of ground states which corresponded to magnetic configurations including non-magnetic, ferromagnetic and antiferromagnetic in different BCC, FCC (Face Centered Cubic) and HCP (Hexagonal Close Packed) lattices. Therefore, the unified approach does not only refer to the magnetic state, as stated in the previous point, but also to the crystal lattice in different elements, since HCP structures are also validated under this approach, making the GUES now applicable to hexagonal lattices.

Therefore, it is not the scope of this work to propose a new interatomic potential, but to modify the GUES to include a non-collinear term, which can include FM and AFM, opening the door to unify the formulation for any magnetic configuration, and at the same time, test this approach with other elements, in addition to Fe. These results will be the starting point for developing interatomic potentials for robust magnetic molecular dynamics simulations.

Results

Unified GUES

The unified formulations for different magnetic configurations are presented hereinafter, along with the magnetic and distance-dependent functions which are therefore introduced (corresponding to previous point 1), and the extension of the GUES to other elements is shown afterwards (corresponding to previous point 2), making use of such unified formulation.

In[19], the parameters of Eq. (3) E_g, V_g, and K_g were defined as:

$$\begin{cases} E_g^i(\boldsymbol{\rho},\boldsymbol{M}) = E_0^i(\boldsymbol{\rho}) + \Phi_E(M_i) + \sum_{j\neq i}^{N} \omega_M\left(\rho_{ij}\right)\psi_E\left(M_i\cdot M_j\right) \\ V_g^i(\boldsymbol{\rho},\boldsymbol{M}) = V_0^i(\boldsymbol{\rho}) + \Phi_V(M_i) + \sum_{j\neq i}^{N} \omega_M\left(\rho_{ij}\right)\psi_V\left(M_i\cdot M_j\right) \\ K_g^i(\boldsymbol{\rho},\boldsymbol{M}) = K_0^i(\boldsymbol{\rho}) + \Phi_K(M_i) + \sum_{j\neq i}^{N} \omega_M\left(\rho_{ij}\right)\psi_K\left(M_i\cdot M_j\right) \end{cases} \quad (4)$$

where the subscript $j\neq i$ represents all neighbor atoms of atom i. It is worth noting that, formally, $j = 1,\ldots,N$ with $j\neq i$ runs over the whole system of N atoms. An interatomic potential derived from the GUES will consider logically the closest atoms and not all atoms in the system. In our previous work, where an interatomic potential was derived only for the ferromagnetic case in Fe, the cutoff distance was for $\rho_{ij} < 40$, which according to Eq. (2) is approximately 7.7 Å for the BCC case, corresponding to 10 nearest neighbors or equivalently around 170 atoms. The functions with 0-subscript are dependent on the distances only, but not on the magnetic moment nor magnetic configuration. It is worth noting that the E_0, V_0 and K_0 parameters does not include any angular dependency, as for instance the Modified Embedded Atom Model (MEAM)[36–38], since the predicted energy by using only distance dependency between pair of atoms in our work provides enough accuracy as it will be shown later (in subheading "Error analysis of the GUES"). The Φ-functions are dependent only on the magnetic moment magnitude M_i of the atom being evaluated i. As pointed out, in the original formulation, these functions were different for the FM and AFM. Similarly occurred with the ψ-functions, which were different in the FM and AFM cases, although in this case, they are multiplied by a function dependent on the distance between atoms i and j. In this revised GUES, both Φ-functions and ψ-functions are now the same for FM and AFM cases. Irrespective of the magnetic function, no orientation was needed as they were different functions or formulations for FM and AFM, and the parameters M_i and M_j were only the magnitude of the magnetic moments $\vec{M}_i$ and $\vec{M}_j$, respectively, but not information about the orientation of the magnetic moment was required. Equation (4) has therefore been reformulated, taking the FM configuration as a base case, where all magnetic moments are aligned, and additional terms for non-collinear magnetic moments must be added. In other words, the formulation in Eq. (4) remains the same for FM, to be consistent with the original results, and the additional terms should be dependent on the angle between different magnetic moments, with the only condition that such terms become 0 for angles equal to 0 (i.e., the FM case). The following formulation responds to such requirements and replaces Eq. (4) to account for any magnetic configuration, rather than only the FM configuration :

$$\begin{cases} E_g^i(\boldsymbol{\rho},\boldsymbol{M}) = E_0^i(\boldsymbol{\rho}) + \Phi_E(M_i) + \sum_{j\neq i}^{N} \omega_M\left(\rho_{ij}\right)\psi_E\left(M_i\cdot M_j\right) + \sum_{j\neq i}^{N} \omega_{nC}\left(\rho_{ij}\right)\Theta_E\left(M_i\cdot M_j\right)\left(\sin\left(\frac{\alpha_{ij}}{2}\right)\right)^2 \\ V_g^i(\boldsymbol{\rho},\boldsymbol{M}) = V_0^i(\boldsymbol{\rho}) + \Phi_V(M_i) + \sum_{j\neq i}^{N} \omega_M\left(\rho_{ij}\right)\psi_V\left(M_i\cdot M_j\right) + \sum_{j\neq i}^{N} \omega_{nC}\left(\rho_{ij}\right)\Theta_V\left(M_i\cdot M_j\right)\left(\sin\left(\frac{\alpha_{ij}}{2}\right)\right)^2 \\ K_g^i(\boldsymbol{\rho},\boldsymbol{M}) = K_0^i(\boldsymbol{\rho}) + \Phi_K(M_i) + \sum_{j\neq i}^{N} \omega_M\left(\rho_{ij}\right)\psi_K\left(M_i\cdot M_j\right) + \sum_{j\neq i}^{N} \omega_{nC}\left(\rho_{ij}\right)\Theta_K\left(M_i\cdot M_j\right)\left(\sin\left(\frac{\alpha_{ij}}{2}\right)\right)^2 \end{cases} \quad (5)$$

where the parameters E_0^i, V_0^i and K_0^i are:

$$\begin{cases} E_0^i(\boldsymbol{\rho}) = \varepsilon_{0,0} + \varepsilon_{0,1}\sum_{j\neq i}^{N} \omega_0\left(\rho_{ij}\right) \\ V_0^i(\boldsymbol{\rho}) = \nu_{0,0} + \nu_{0,1}\sum_{j\neq i}^{N} \omega_0\left(\rho_{ij}\right) \\ K_0^i(\boldsymbol{\rho}) = \kappa_{0,0} + \kappa_{0,1}\sum_{j\neq i}^{N} \omega_0\left(\rho_{ij}\right) \end{cases} \quad (6)$$

and ω_0 and ω_M are distance-dependent functions, which is common for the three parameters functions E_0^i, V_0^i and K_0^i are as it can be seen in Eqs. (5) and (6). The values and physical meaning of the parameters $\varepsilon_{0,0}$, $\varepsilon_{0,1}$, $\nu_{0,0}$, $\nu_{0,1}$, $\kappa_{0,0}$ and $\kappa_{0,1}$ is explained later (in subheading "Non-magnetic contributions of the GUES"). The new ω_{nC} in Eq. (5) (as compared to initial GUES formulation) is another distance-dependent function, which scales the influence of close atoms, decreasing with the interatomic distance. The Θ-functions, also new in this work, are also dependent on the magnitude of the magnetic moments M_i and M_j, of atoms i and j, respectively. The angle between magnetic moments $\vec{M}_i$ and $\vec{M}_j$ is denoted α_{ij}, and it is introduced in the term $\sin\left(\frac{\alpha_{ij}}{2}\right)^2$. This term is the simplest function to account for magnetic angular dependence, allowing also for the transition between the previous FM and AFM formulations at[19] and incorporating at the same time non-collinear contributions. In other words, for the FM case, the collinear magnetic moments do not contribute to the non-collinear extra terms, as this term is equal to 0. Therefore, for pure collinear FM configurations, the formulation is consistent with the previous interatomic potential. Also, in the AFM configuration, only half of the atoms contribute to the non-collinear terms, where previous Ψ-functions in the AFM case at[19] (which were initially different in our previous work to the Ψ-functions for the FM case) arise now as the addition of current Ψ-functions and Θ-functions, multiplied by the corresponding distance dependence functions ω_M and ω_{nC}, respectively, in their respective atomic neighbors. For the non-collinear (fully disordered magnetic moments), any atom can actually contribute to each other in the non-collinear term. With this, the AFM configuration is, mathematically, a particular case of the non-collinear configuration.

In addition to this, this term can be expressed as $sin\left(\frac{\alpha_{ij}}{2}\right)^2 = \frac{1}{2}(1-\cos(\alpha_{ij}))$, which can be related to the Heisenberg model description of the angular contribution between different spins[15]. In such a model, that contribution of the energy is multiplied by the distance-dependent exchange interactions (usually denoted as J_{ij}), which can be related to the distance dependence functions ω_{nC} in Eq. (5). Therefore, the proposed formulation is consistent with Heisenberg model, but also with the Ginzburg-Landau approximation[39] which describes the FM contribution to the energy in the form of even polynomials, as the Ψ-functions actually behave in our approach.

Error analysis of the GUES

For this subheading, it is important to notice the difference between the GUES and a magnetic interatomic potential (MIP) based on the GUES. The GUES is a formulation, independent of the MIP, which describes the energy of a system. The MIP is the set of motion equations that allows for MD simulations. In the same way that a Heisenberg-Landau Hamiltonian is the formulation for the energy, and a many-body potential based on the Heisenberg-Landau Hamiltonian[11], is the actual interatomic potential for MD simulations. Also, the Embedded Atom Model is the formulation, and the Finnis-Sinclar potentials are the actual interatomic potentials[40].

With this in mind, the distance-dependent functions $\omega_0(\rho_{ij})$, $\omega_M(\rho_{ij})$ and $\omega_{nC}(\rho_{ij})$ do not need to be described at this point to prove the validity of the GUES for different elements (they would need to be developed for MD simulations). The database is constructed in a way that it can be separated in Eq. (5) to allow for energy calculations in different structures. For a certain structure, cubic or hexagonal, with lattice parameters $\langle a, b, c\rangle$ and a fixed and constant magnitude of the magnetic moments with the AFM configuration as described in the previous subheading with alternate spin up—spin down layers in the (0,0,1) or (0,0,0,1) for cubic and hexagonal-based lattices, respectively, Eq. (5) can be rewritten as:

$$\begin{cases} E_g^i(\boldsymbol{\rho},\boldsymbol{M}) = \varepsilon_{0,0} + \varepsilon_{0,1}\Omega_0 + \Phi_E(M_i) + \Omega_M\psi_E\left(M_i^2\right) + \Omega_{nC}\Theta_E\left(M_i^2\right)\left(\sin\left(\frac{\alpha}{2}\right)\right)^2 \\ V_g^i(\boldsymbol{\rho},\boldsymbol{M}) = \nu_{0,0} + \nu_{0,1}\Omega_0 + \Phi_V(M_i) + \Omega_M\psi_V\left(M_i^2\right) + \Omega_{nC}\Theta_V\left(M_i^2\right)\left(\sin\left(\frac{\alpha}{2}\right)\right)^2 \\ K_g^i(\boldsymbol{\rho},\boldsymbol{M}) = \kappa_{0,0} + \kappa_{0,1}\Omega_0 + \Phi_K(M_i) + \Omega_M\psi_K\left(M_i^2\right) + \Omega_{nC}\Theta_K\left(M_i^2\right)\left(\sin\left(\frac{\alpha}{2}\right)\right)^2 \end{cases} \tag{7}$$

where

$$\begin{cases} \Omega_0 = \sum_{j\neq i}^{N} \omega_0\left(\rho_{ij}\right) \\ \Omega_M = \sum_{j\neq i}^{N} \omega_M\left(\rho_{ij}\right) \\ \Omega_{nC} = \sum_{j\in\Gamma} \omega_{nC}\left(\rho_{ij}\right) \end{cases} \tag{8}$$

and Γ denotes the neighbors with different spin orientation to atom i, with the spin non-collinear angle denoted α. For a spin up atom i, the angle α in the alternate spin up—spin down layers in the (0,0,1) or (0,0,0,1) for cubic and hexagonal-based lattices, respectively, will be 0 for all other spin up atoms, and 180 ° for all spin down atoms. With this, the atoms with the same spin orientation to atom i will not have a contribution to the non-collinear term, as they are multiplied by $(\sin(0))^2$. Therefore, the fitted values of Ω_{nc} are valid for any magnetic configuration from FM to AFM, as described in the database (B2-like, $L1_0$-like, and B_h-like structures for cubic and hexagonal, respectively) with the α angle rotating between 0 ° and 180 °.

Therefore, the expressions of ω_0, ω_M and ω_{nC} are not the central point in this paper, since they are actually the functions needed for the molecular dynamics simulations, and will be considered in subsequent works. The expression for Ω_0, Ω_M, Ω_{nC} can be then expressed as a function of $\langle b/a, c/a\rangle$, without the need of ω_0, ω_M and ω_{nC}, as well as Φ-, ψ- and Θ-magnetic functions can be expressed in terms of M_i^2 since for these functions, the magnetic moment magnitudes are constant for each case, being in that case $\boldsymbol{M} = \langle\vec{M}_i, \vec{M}_i, \vec{M}_i, \ldots, \vec{M}_i, \ldots\rangle$.

From the original proposal of the GUES in ref. 19, it was proved that, in the case of Fe, for any fixed lattice and magnetic magnitude and configuration, there exist values of $\langle E_g, V_g, K_g\rangle$ which describe the variation of the energy by means of the atomic volume, following Eq. (1). These values have been fitted in this work by all the elements considered, namely, Co, Cr, Fe, Mn and Ni, for all cubic and hexagonal based lattices, with NM, FM and AFM configurations. The predictions of the GUES by using this fitting are shown in some specific cases in Fig. 1 for NM, FM, and AFM magnetic configurations, as indicated in the figure. The figures show the DFT calculated energies, and the corresponding function in Eq. (1), each of them calculated after the corresponding fitting of $\langle E_g, V_g, K_g\rangle$. Note that any other case non-displayed in the figure (for the sake of clarity) has been checked carefully and follows the same trend, concluding that, for any lattice and magnetic configuration, there exist values of $\langle E_g, V_g, K_g\rangle$ which capture the variation of the energy by means of the atomic volume.

The complete comparison of the predictions for all data is shown in a scatter plot with DFT data vs. GUES prediction in Fig. 2 by numerically fitting individually for each lattice and magnetic moment the corresponding set of E_g, V_g and K_g parameters (including the data shown in Fig. 1). The results support the validity of the GUES with an $RMSE = 4.22\ 10^{-6}$ eV (Root Mean Squared Error) corresponding to all data considered, showing good agreement between DFT and GUES prediction.

Non-magnetic contributions of the GUES

Once the reliability of the GUES in predicting energies is proven, it is now the turn to analyse the $\langle E_g, V_g, K_g\rangle$ behavior of each case. The non-magnetic interactions are considered first, which are the simplest case, and allow constructing the subsequent magnetic contributions. It is expressed in terms of Ω_0 for each of the elements (Eq. (8)), and correspond to the DFT data with magnetic magnitude equal to 0. The fitted $\left\langle E_g, V_g, K_g\right\rangle$ parameters which have been used in Fig. 1 (top illustration) using Eq. (1) for Co, Cr, Fe, Mn, and Ni, are now displayed as a function of the ratios $\langle b/a, c/a\rangle$ for cubic- and hexagonal-base lattices, whenever it corresponds. The results are displayed in Fig. 3 for all elements, where the top row corresponds to cubic structures and the bottom row corresponds to hexagonal lattices. The fitted values for Ω_0 are in the supplementary material for all elements. It is worth noting that Ω_0 functions are not uniquely defined, since the non-magnetic contribution is scaled with $\varepsilon_{0,0}$, $\varepsilon_{0,1}$, $\nu_{0,0}$, $\nu_{0,1}$, $\kappa_{0,0}$, and $\kappa_{0,1}$ parameters, which are shown in Table 1. In this work, the Ω_0 selected so that its value in the FCC lattice $\langle b/a = 1, c/a = \sqrt{2}\rangle$ equals to 0, and in the BCC lattice $\langle b/a = 1, c/a = 1\rangle$ equals to 1. Therefore, the $\varepsilon_{0,0}$ is the ground state energy for non-magnetic configuration of the FCC lattice, whereas $\varepsilon_{0,0} + \varepsilon_{0,1}$ is the ground state energy for non-magnetic configuration of the BCC lattice. Equivalently, $\nu_{0,0}$ is the ground state volume of BCC, and $\nu_{0,0} + \nu_{0,1}$ is the ground state of FCC. On the other hand, $\kappa_{0,0}$ is related to the bulk modulus B_g ground state[19] since the following relationship applies:

$$B_g(\rho, M) = -\frac{E_g(\rho, M)V_g(\rho, M)}{K_g(\rho, M)^2} \tag{9}$$

which, for the BCC case, is $B_g = -\frac{\varepsilon_{0,0}\nu_{0,0}}{\kappa_{0,0}^2}$, while for the FCC case its bulk modulus ground state is $B_g = -\frac{(\varepsilon_{0,0}+\varepsilon_{0,1})(\nu_{0,0}+\nu_{0,1})}{(\kappa_{0,0}+\kappa_{0,1})^2}$. Figure 3 shows a relatively similar behavior of Co, Fe, Mn, and Ni in the non-magnetic state in both cubic and hexagonal lattices, where Cr is clearly dissimilar to the other elements.

Self-magnetic contribution of the GUES

Following the sequence of functions in Eq. (5), the magnetic functions $\Phi_E(M)$, $\Phi_V(M)$, and $\Phi_K(M)$ for all elements are now considered. These functions account for the contribution to the energy of an atom, irrespective of the magnetic state of the rest of the atoms or their interaction with such an atom. Particularly, it represents the nature of the magnetic moment, and not the magnetic ordering of the system, resembling the on-site energy in the Heisenberg-Landau Hamiltonian[11]. In other words, in a simulation cell with all magnetic moments equal to 0 except for an atom, such an atom would still induce an effect on E_g, V_g, and K_g, and therefore on the energy of the system. Further, this contribution is also independent of the distances ρ between such an atom and the other atoms, or in other words, the variation on E_g, V_g, and K_g induced by the change in magnetic moment of an atom is

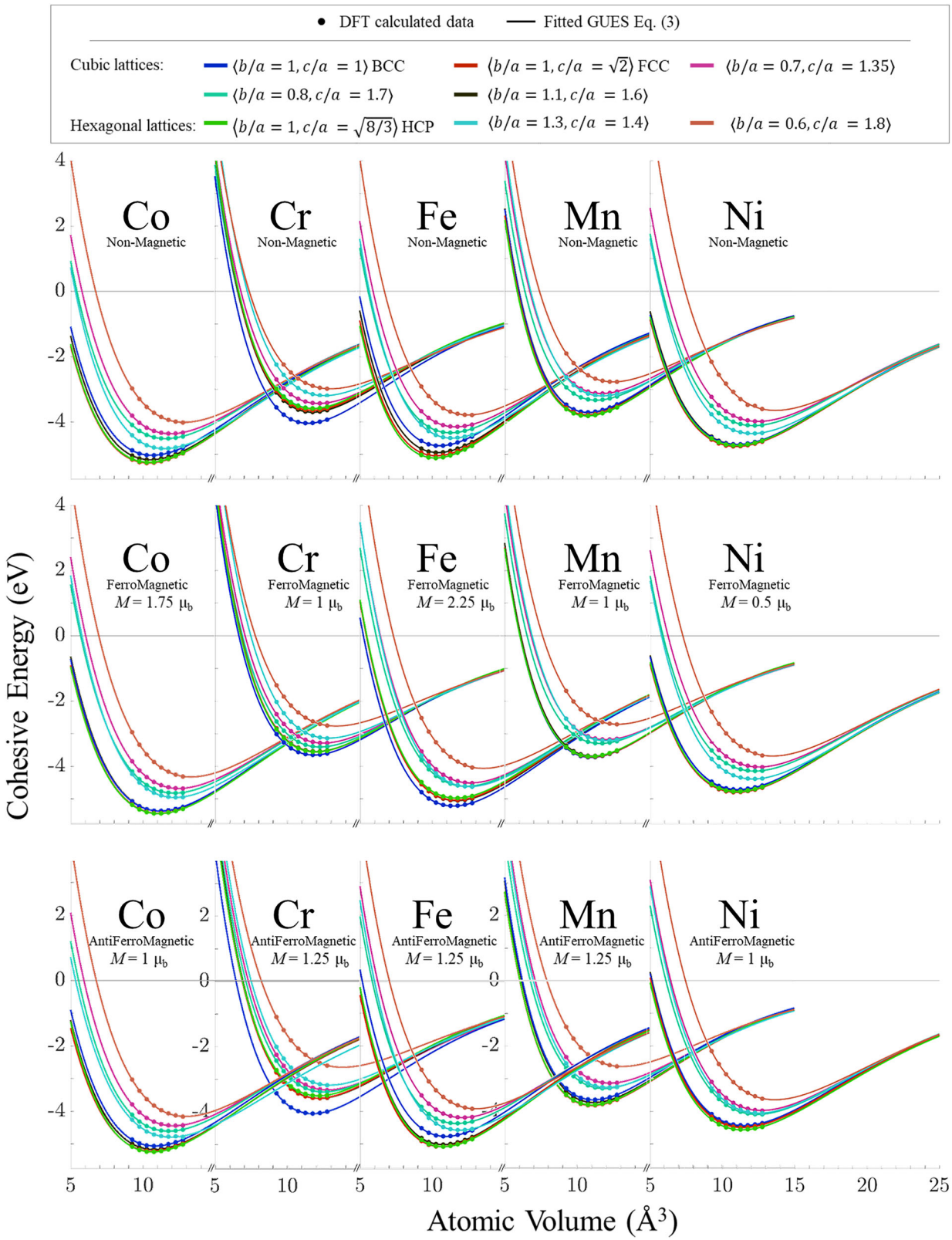

Fig. 1 | GUES description of the volume-energy variation of Co, Cr, Fe, Mn, and Ni for NM, FM, and AFM. Cohesive energy and fitting to the Universal Equation of States as shown in Eq. (3) for different element, crystal lattices, and magnetic configurations, as indicated in the figure. Note that *x*-axis is shifted and overlapped for different pictures. Legend is common for all illustrations. BCC, FCC, and HCP corresponding structures are indicated in the legend.

the same, irrespective of the crystal lattice and volume, since ρ and V are not part of Φ-functions.

Figure 4 shows all Φ-functions for all elements. In Fig. 4a, the $\Phi_E(M)$ function is depicted, showing its clear influence on the ferromagnetic behavior of each of the elements. For instance, Co and Fe display minimum values of $\Phi_E(M)$ around 1.64 μ_b and 2.35 μ_b, respectively, which is very close to the magnitude of the magnetic moment providing the minimum energy in ferromagnetic

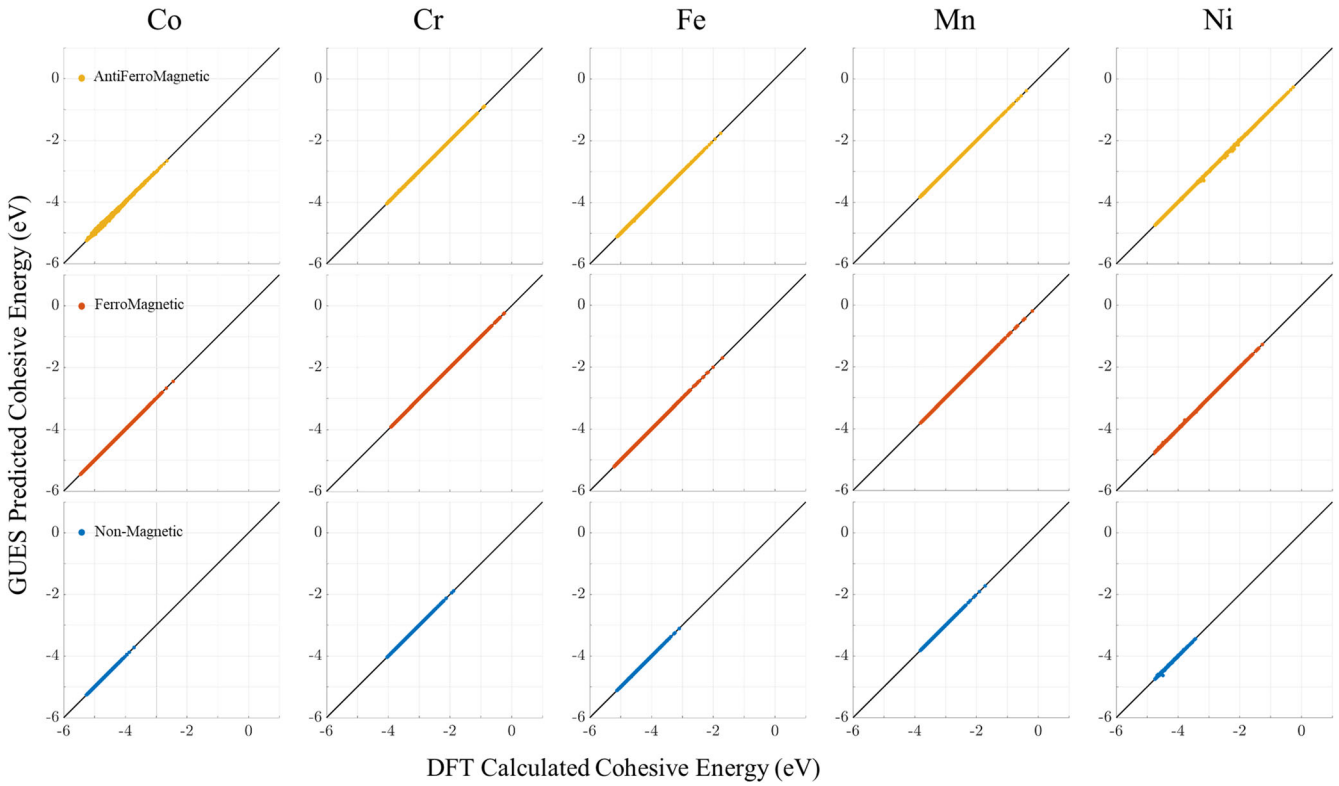

Fig. 2 | Prediction of the energy with the GUES for Co, Cr, Fe, Mn, and Ni, for NM, FM, and AFM. DFT calculated cohesive energy vs. GUES predicted cohesive energy with fitted E_g, V_g, and K_g, for Co, Cr, Fe, Mn, and Ni, in non-magnetic, ferromagnetic, and antiferromagnetic for all cubic- and hexagonal-based lattices. The RMSE = 4.22 10^{-6} eV correspond to all data considered.

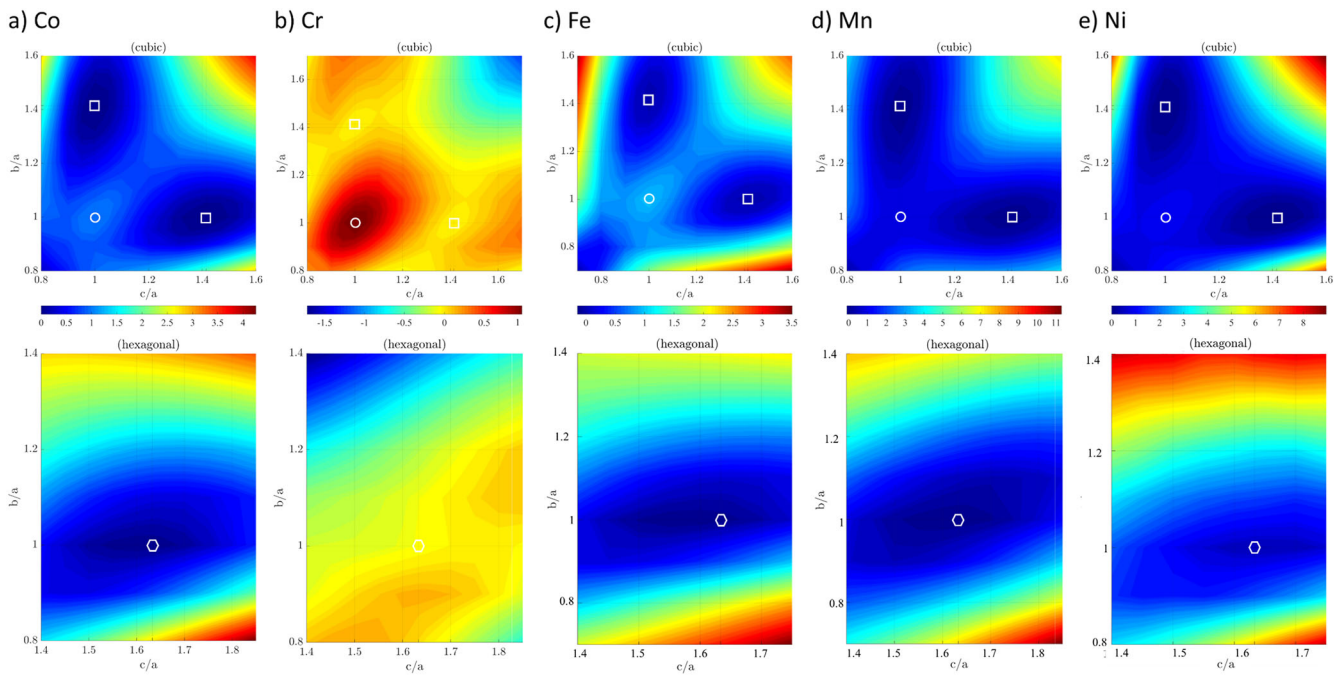

Fig. 3 | Distance dependent Ω_0 functions of the GUES. Ω_0 functions (Eq. (8)) describing the non-magnetic contribution for **a** Co, **b** Cr, **c** Fe, **d** Mn, and **e** Ni. Solid white dots indicate the $\Omega_0 = 1$ value, which correspond to BCC lattice, solid square dots indicate the $\Omega_0 = 0$ which correspond to FCC lattice, and solid hexagonal dots corresponds to perfect HPC lattice.

configuration, which occurs at 1.75 μ_b and at 2.25 μ_b, respectively. Note that the minimum energy (and the corresponding magnitude of the magnetic moment) may not be calculated in the DFT database since the calculations are performed in fixed *c/a* and *b/a* ratios, volumes, and magnetic moments. Also, Ni shows a minimum value of $\Phi_E(M)$ at 0.57 μ_b, whereas the minimum energy of the DFT database lies in 0.5 μ_b for the ferromagnetic case. On the other hand, Mn and Cr show mainly positive values of $\Phi_E(M)$, increasing in this way the energy of the system

Table 1 | Parameters of the non-magnetic contribution to E_g, V_g, and K_g for all elements considered, as expressed in Eq. (7)

Parameter	Co	Cr	Fe	Mn	Ni
$\varepsilon_{0,0}$ (eV)	−5.2424	−3.6559	−5.0637	−3.7822	−4.7602
$\varepsilon_{0,1}$ (eV)	$2.0240 \cdot 10^{-1}$	$-3.3921 \cdot 10^{-1}$	$3.3743 \cdot 10^{-1}$	$9.2740 \cdot 10^{-2}$	$6.5844 \cdot 10^{-2}$
$\nu_{0,0}$ (Å^3)	10.2500	11.8260	10.1790	10.6160	10.9150
$\nu_{0,1}$ (Å^3)	$4.8235 \cdot 10^{-1}$	$-6.5017 \cdot 10^{-1}$	$5.8467 \cdot 10^{-1}$	$1.7742 \cdot 10^{-1}$	$1.6214 \cdot 10^{-1}$
$\kappa_{0,0}$ (Å^3)	6.1435	5.1831	5.6697	4.8012	6.4211
$\kappa_{0,1}$ (Å^3)	$1.8644 \cdot 10^{-2}$	$-1.5159 \cdot 10^{-1}$	$7.0577 \cdot 10^{-3}$	$1.9911 \cdot 10^{-2}$	$-2.0232 \cdot 10^{-2}$

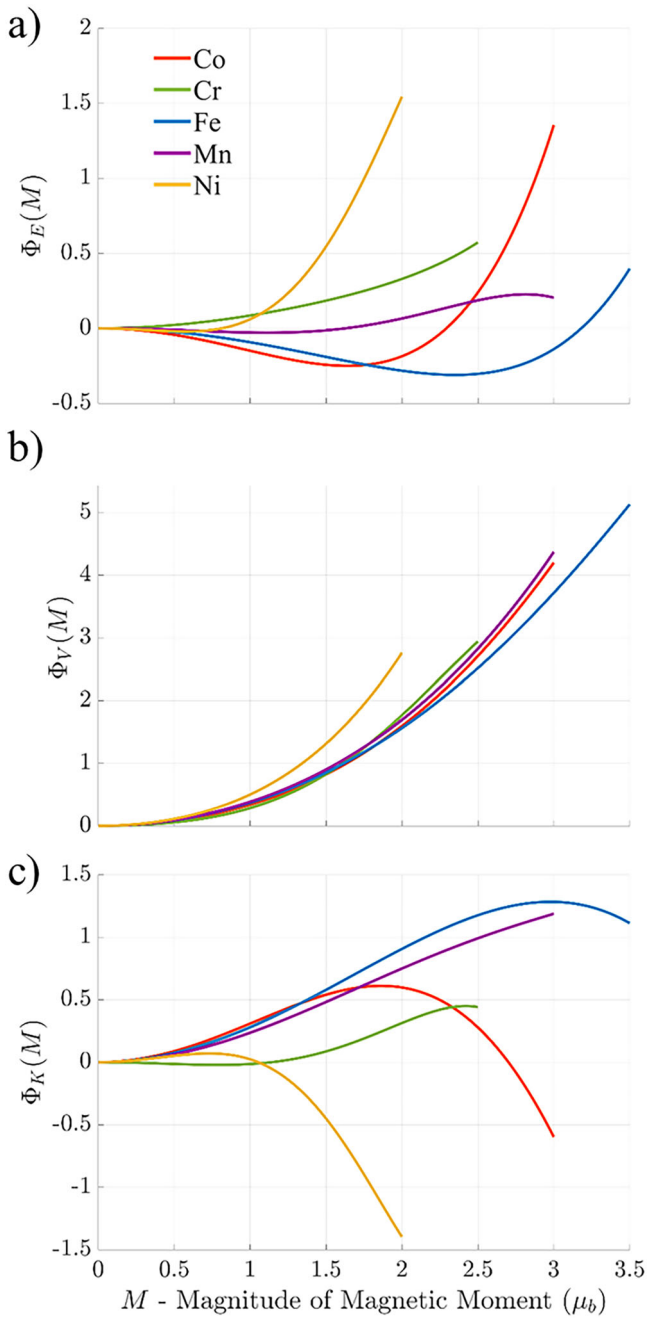

Fig. 4 | Magnetic dependent Φ-functions of the GUES. Magnetic functions **a** Φ_E, **b** Φ_V and **c** Φ_K for Co, Cr, Fe, Mn and Ni. Note that the legend is common for all figures and is indicated only in (**a**), and similarly, the *x*-axis is common for all figures but is only indicated in (**c**).

for magnetic configurations, in agreement with the minimum energy for ferromagnetic configuration, which occurs for $M = 0$, i.e., non-magnetic. Similarly, $\Phi_V(M)$, which stands for the volume behavior with magnetic moment, has a very constantly increasing value with magnetic moment for all elements. This means that the increase of magnitude of the magnetic moment also increases the volume at which the minimum energy occurs. This is a common feature in the DFT database for all elements considered, where indeed the non-magnetic ground state has a lower volume than magnetic configurations. Other previous results confirm this tendency[41–45], where volume-dependent energy shows also larger volumes for FM and AFM configurations, as compared to NM state. The influence of $\Phi_K(M)$ is much more subtle since it is related to the bulk modulus B_g through Eq. (9). It is worth noting that every lattice (defined by the set of distances ρ) and magnetic moment M has a corresponding bulk modulus. Following this equation, the influence of $\Phi_K(M)$ on the bulk modulus is much more complex and related also to $\Phi_E(M)$ and $\Phi_V(M)$.

The functional forms of Φ_E, Φ_V, and Φ_K were described in our previous paper[19], and are expressed in terms of a Taylor series expansion of an unknown even function. Therefore, they are even polynomials as a function of the magnitude of the magnetic moment M. This functional form, share the functional form of the Ginzburg-Landau approximation which is a sum of a second-order and fourth-order terms[25,39], which describes the Stoner model by relating the order parameter (magnetization) to the microscopic properties of the Stoner model, such as the band structure and exchange interactions. It was shown in our previous paper[19] that order 4 may be sufficient for FM BCC Fe, or small deviations, but it could not cover all the different lattices, demanding therefore additional terms. In agreement to our initial conclusion, we observe indeed that at including the extended database in hexagonal lattices Fe, as well as all cubic and hexagonal lattices in Co, Cr, Mn, and Ni, the order 2 and order 4 terms cannot fit the DFT calculations, and they need at least the M^6 additional term. The magnetic functions proposed here, as well as the Ginzburg–Landau model, suggest the existence of unknown close functions, whose series expansion coefficients are the actual parameters fitted in Eqs. (10 and 11), as well as the so-called α and β parameters, multipliers of M^2 and M^4 respectively of Ginzburg–Landau model[24,39].

$$\begin{cases} \Phi_E(M) = \varepsilon^{\Phi}_{2,0} M^2 + \varepsilon^{\Phi}_{4,0} M^4 + \varepsilon^{\Phi}_{6,0} M^6 + O(M^8) \\ \Phi_V(M) = \nu^{\Phi}_{2,0} M^2 + \nu^{\Phi}_{4,0} M^4 + \nu^{\Phi}_{6,0} M^6 + O(M^8) \\ \Phi_K(M) = \kappa^{\Phi}_{2,0} M^2 + \kappa^{\Phi}_{4,0} M^4 + \kappa^{\Phi}_{6,0} M^6 + O(M^8) \end{cases} \tag{10}$$

The ε, ν, κ parameters for Φ for all elements are displayed in Table 2.

Ferromagnetic contribution of the GUES

A corresponding analysis of the one performed for Ω_0 in Fig. 3 can be now performed for the Ω_M distance-dependent function, which, together with the ψ- functions, accounts for the contribution of the magnitudes of the magnetic moments, corresponding to a ferromagnetic configuration. It is worth noting that, indeed, the case of ferromagnetism is not defined by only the contribution of Ω_M and the ψ- functions, as explained above, since the

Table 2 | Values of the ε, ν, κ parameters for Φ functions for Co, Cr, Fe, Mn and NiParameter (units)

	Co	Cr	Fe	Mn	Ni
$\varepsilon^{\Phi}_{2,0}$ (eV/μ_b^2)	$-1.7858 \cdot 10^{-1}$	$1.1071 \cdot 10^{-1}$	$-9.6977 \cdot 10^{-2}$	$-4.4597 \cdot 10^{-2}$	$-1.3302 \cdot 10^{-1}$
$\varepsilon^{\Phi}_{4,0}$ (eV/μ_b^4)	$3.0640 \cdot 10^{-2}$	$-1.0951 \cdot 10^{-2}$	$5.0060 \cdot 10^{-3}$	$1.9821 \cdot 10^{-2}$	$2.1430 \cdot 10^{-1}$
$\varepsilon^{\Phi}_{6,0}$(eV/μ_b^6)	$6.7084 \cdot 10^{-4}$	$5.1696 \cdot 10^{-4}$	$4.5600 \cdot 10^{-4}$	$-1.4126 \cdot 10^{-3}$	$-2.1127 \cdot 10^{-2}$
$\nu^{\Phi}_{2,0}$ (Å^3/μ_b^2)	$1.5877 \cdot 10^{-1}$	$1.1052 \cdot 10^{-1}$	$1.8237 \cdot 10^{-1}$	$2.0098 \cdot 10^{-1}$	$2.1455 \cdot 10^{-1}$
$\nu^{\Phi}_{4,0}$ (Å^3/μ_b^4)	$1.1469 \cdot 10^{-2}$	$5.3192 \cdot 10^{-2}$	$3.9790 \cdot 10^{-3}$	$4.6078 \cdot 10^{-3}$	$3.6169 \cdot 10^{-2}$
$\nu^{\Phi}_{6,0}$ (Å^3/μ_b^6)	$-3.5579 \cdot 10^{-4}$	$-4.7307 \cdot 10^{-3}$	$-1.4419 \cdot 10^{-4}$	$8.4403 \cdot 10^{-5}$	$-8.9006 \cdot 10^{-4}$
$\kappa^{\Phi}_{2,0}$ (Å^3/μ_b^2)	$1.4354 \cdot 10^{-1}$	$-9.4567 \cdot 10^{-3}$	$1.4100 \cdot 10^{-1}$	$1.3117 \cdot 10^{-1}$	$1.3611 \cdot 10^{-1}$
$\kappa^{\Phi}_{4,0}$ (Å^3/μ_b^4)	$-1.9952 \cdot 10^{-2}$	$2.0002 \cdot 10^{-2}$	$-6.3934 \cdot 10^{-3}$	$-1.3339 \cdot 10^{-2}$	$-1.4006 \cdot 10^{-1}$
$\kappa^{\Phi}_{6,0}$ (Å^3/μ_b^6)	$2.6598 \cdot 10^{-5}$	$-1.5605 \cdot 10^{-3}$	$-1.3328 \cdot 10^{-4}$	$7.9923 \cdot 10^{-4}$	$1.5588 \cdot 10^{-2}$

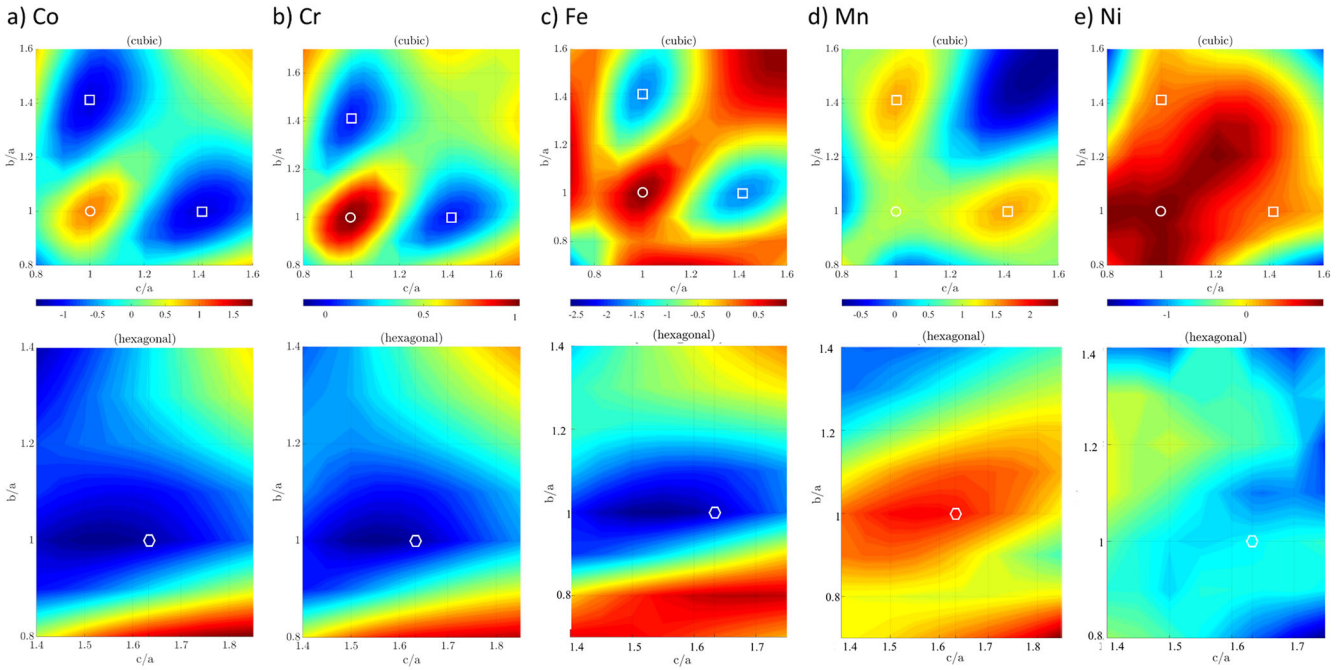

Fig. 5 | Distance dependent Ω_M functions of the GUES. Ω_M functions (Eq. (8)) describing the magnitude of the magnetic contribution for **a** Co, **b** Cr, **c** Fe, **d** Mn, and **e** Ni. Solid white dots indicate the $\Omega_M = 1$ value which correspond to BCC lattice, solid square dots indicate FCC lattice, and solid hexagonal dots corresponds to perfect HPC lattice.

magnitude of the magnetic moment of each atom deeply modifies the energy of the system, independently of the orientation of the magnetic moment of the other atoms.

The Ω_M functions are shown in Fig. 5 for all elements and the fitted values for Ω_M are in the supplementary material for all elements. As in the case of Ω_0, the Ω_M functions are not uniquely defined since they are always multiplied by ψ- functions, and therefore they can be scaled accordingly to the ψ- functions. We have chosen $\Omega_M = 1$ for the BCC case as in the case of Ω_0. Note that, for the Ω_M case, its value in the FCC cannot be scaled to 0 as in the case of Ω_0. In this case, Co, Cr, and Fe show similar behavior, which does not mean that the ferromagnetic behavior must be similar, since this goes in combination with ψ- functions. On the other side, Mn and Ni have no relationship with the other elements. Figure 6 shows the corresponding ψ-functions, which together with Ω_M finally define the ferromagnetic configuration. There are no simple conclusions to extract from these functions, which show complex and different behaviors. Nevertheless, an analysis of the contribution of each function is performed later.

The functional forms of Ψ_E, Ψ_V and Ψ_K were described in our previous paper[19], and are expressed in terms of a Taylor series expansion of an unknown even function. This proposed formulation is consistent with the Heisenberg-Landau Hamiltonian used for magnetic cluster expansion simulations, where the non-magnetic contribution of the GUES is related to the NM cluster expansion coefficients, while the Φ-functions correspond to the Landau coefficients and the Ψ-functions, represent the lattice magnetic configuration described by the interlattice-site Heisenberg magnetic interaction parameters[11].

$$\begin{cases} \Psi_E(M) = \varepsilon^{\Psi}_{2,0}M^2 + \varepsilon^{\Psi}_{4,0}M^4 + \varepsilon^{\Psi}_{6,0}M^6 + O(M^8) \\ \Psi_V(M) = \nu^{\Psi}_{2,0}M^2 + \nu^{\Psi}_{4,0}M^4 + \nu^{\Psi}_{6,0}M^6 + O(M^8) \\ \Psi_K(M) = \kappa^{\Psi}_{2,0}M^2 + \kappa^{\Psi}_{4,0}M^4 + \kappa^{\Psi}_{6,0}M^6 + O(M^8) \end{cases} \quad (11)$$

The ε, ν, κ parameters for Ψ functions for all elements are displayed in Table 3.

Non-collinear contribution of the GUES

The next Figs. 7 and 8 show the Ω_{nC} distance-dependent functions and θ magnetic-dependent functions, which capture the contribution for non-

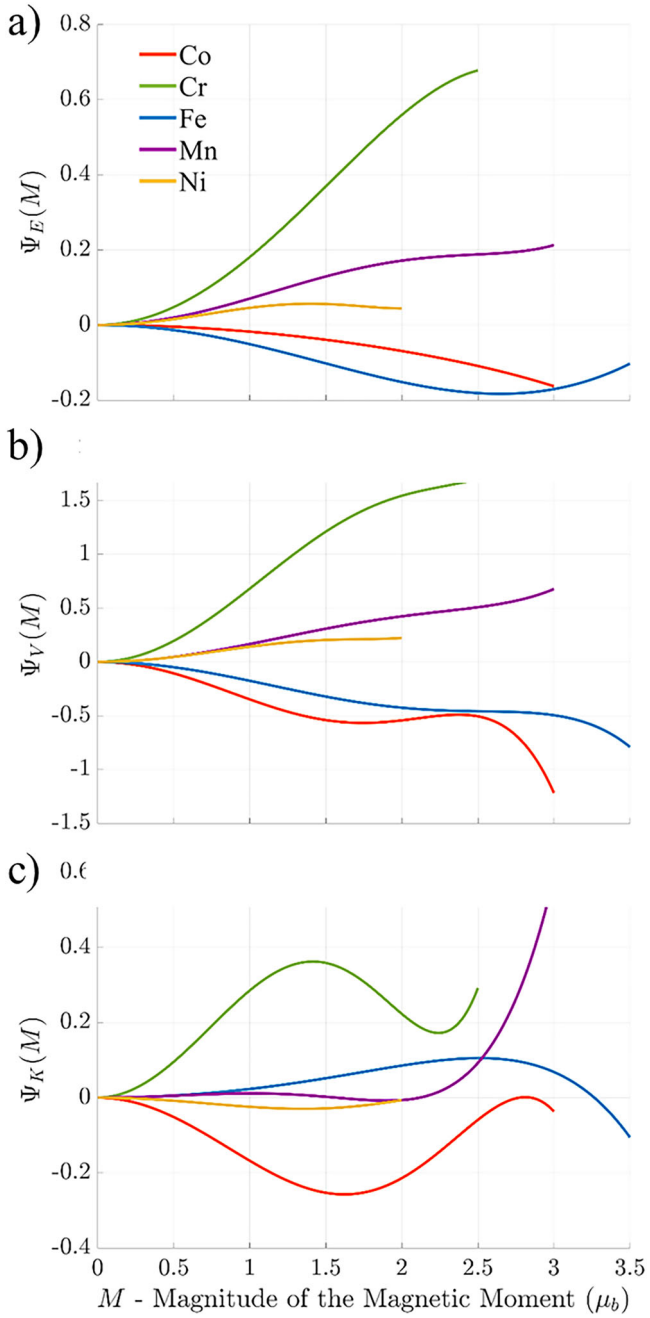

Fig. 6 | Magnetic dependent Ψ-functions of the GUES. Magnetic functions **a** Ψ_E, **b** Ψ_V, and **c** Ψ_K for Co, Cr, Fe, Mn and Ni. Note that the legend is common for all figures and is indicated only in (**a**), and similarly, the x-axis is common for all figures but is only indicated in (**c**).

collinear magnetic moments, in the same way as previous figures (Figs. 5 and 6) showed for the collinear magnetic moments. The fitted values for Ω_{nC} are in the supplementary material for all elements. Similarly, as for previous omegas, Ω_{nC} is always scaled to obtain $\Omega_{nC} = 1$ for the BCC case. Note that, for the Ω_{nC} case, its value in the FCC cannot be scaled to 0 as in the case of Ω_0. It is worth noting that Ω_{nC} and θ are indeed fitted for AFM configuration, where the non-collinearity is given by the angle α_{ij} between magnetic moments with different orientations. Although the non-collinearity is indeed driven by such angle, the magnitude of the non-collinear contribution is defined Ω_{nC} and θ functions.

With this, it is easy to see in the case of Cr, when both Figs. 7 and 8 are combined, that Cr has a strong antiferromagnetic contribution for BCC, since Ω_{nC} has its maximum value for BCC whereas Θ_E is strongly negative, explaining in this way the antiferromagnetic behavior of Cr in its global ground state, which has −4.05 eV at 1.5 μ_b. This contrasts with the energy of the ferromagnetic configuration of BCC, which is −3.37 eV of the ferromagnetic contribution due to the positive values of Ψ_E at the same magnitude of the magnetic moment. The same effect occurs for Mn, due to positive values of Ψ_E and negative values of Θ_E, providing a cohesive energy of −3.79 eV for ferromagnetic configuration and −3.83 eV for antiferromagnetic configuration in the BCC lattice. The difference between both magnetic configurations is lower, in concordance with the behavior of Ψ_E and Θ_E in Mn (see Figs. 6 and 8). For the same reason, the positive values of Θ_E for Co, Fe, and Ni suggest that the AFM configuration will not show lower values than the ferromagnetic configuration, as indeed occurs.

Also, the behavior of Θ_V (responsible for the volume of antiferromagnetic configuration), shows a lower volume for the BCC lattice for antiferromagnetic configuration than the non-magnetic configuration for Cr and Mn, since this occurs for Cr at 11.75 Å^3 for the non-magnetic configuration and 11.25 Å^3 for the antiferromagnetic configuration. In the case of Mn, the lower energy of BCC for non-magnetic occurs at 11.25 Å^3 and 10.75 Å^3 for the antiferromagnetic configuration.

The functional forms of θ_E, θ_V and θ_K are expressed in terms of a Taylor series expansion of an unknown even function and can be seen in Eq. (12). Therefore, they are even polynomials as a function of the magnitude of the magnetic moment M. The order 6 of the exponent is selected since additional terms does not provide significant improvement on the fitting, avoiding also overfitting of the functions.

$$\begin{cases} \theta_E(M) = \varepsilon^{\theta}_{2,0}M^2 + \varepsilon^{\theta}_{4,0}M^4 + \varepsilon^{\theta}_{6,0}M^6 + O(M^8) \\ \theta_V(M) = \nu^{\theta}_{2,0}M^2 + \nu^{\theta}_{4,0}M^4 + \nu^{\theta}_{6,0}M^6 + O(M^8) \\ \theta_K(M) = \kappa^{\theta}_{2,0}M^2 + \kappa^{\theta}_{4,0}M^4 + \kappa^{\theta}_{6,0}M^6 + O(M^8) \end{cases} \quad (12)$$

The ε, ν, κ parameters for θ functions for all elements are displayed in Table 4:

Factor analysis and predictability of the GUES

This previous analysis, and the contribution of each term of Eq. (7) can be also visualized by means of the factor analysis in Fig. 9. In this figure, it is shown the values for E_g. V_g and K_g of the non-magnetic term of Eq. (7) due to Ω_0 and the corresponding $\varepsilon_{0,0}$, $\varepsilon_{0,1}$, $\nu_{0,0}$, $\nu_{0,1}$,$\kappa_{0,0}$ and $\kappa_{0,1}$ values, which are shown with black dots at $M = 0$ for all cubic and hexagonal lattices. Then, the magnetic term due to Φ-functions with blue dots, only dependent on the magnitude of the magnetic momenta and it is insensitive to magnetic ordering, without influence of other atoms, since it is independent of the lattice, and therefore with the same value of any lattice, with only variation with respect to magnitude of the magnetic moment. It is followed by the contribution of the Ω_M·Ψ-functions, which is dependent on the magnitude of the magnetic moment and the lattice, which is shown with an area in red color, covering all lattices for each magnitude of the magnetic moment. Finally, the Ω_{nC}·Θ-functions contribution for the non-collinear configuration, which is shown with a green colored area, also covers different lattices. In the figure, the images (a–e) are the E_g factor contributions for Co, Cr, Fe, Mn and Ni, the images (f–k) are the V_g factor contributions for Co, Cr, Fe, Mn, and Ni, and images (l–p) are the K_g factor contributions for Co, Cr, Fe, Mn, and Ni, respectively. Note that the maximum values of the magnetic moments vary in each element and magnetic configuration, since the DFT convergence fails for lattices and configurations far from equilibrium, and are discarded from the analysis.

From this factor analysis, it is clear that the energy of a system (through the values of E_g. V_g, and K_g) is mainly defined by the non-magnetic configuration, and slightly varies by the different magnetic configurations. The second term in importance is due to the self-magnetic effect, i.e., the magnitude of the magnetic moment of each atom (shown in blue color), irrespective of the lattice and spin orientation of the other

Table 3 | Values of the ε, ν, κ parameters for Ψ functions for Co, Cr, Fe, Mn, and Ni

Parameter (units	Co	Cr	Fe	Mn	Ni
$\varepsilon^{\Psi}_{2,0}$ (eV/μ_b^2)	$-1.7947 \cdot 10^{-2}$	$2.3084 \cdot 10^{-1}$	$-7.2440 \cdot 10^{-2}$	$6.8071 \cdot 10^{-2}$	$6.9126 \cdot 10^{-2}$
$\varepsilon^{\Psi}_{4,0}$ (eV/μ_b^4)	$3.0857 \cdot 10^{-4}$	$-1.9654 \cdot 10^{-2}$	$9.2814 \cdot 10^{-3}$	$-1.0339 \cdot 10^{-2}$	$-2.6326 \cdot 10^{-2}$
$\varepsilon^{\Psi}_{6,0}$(eV/μ_b^6)	$-3.6364 \cdot 10^{-5}$	$5.5721 \cdot 10^{-4}$	$-3.5404 \cdot 10^{-4}$	$5.4950 \cdot 10^{-4}$	$2.9519 \cdot 10^{-3}$
$\nu^{\Psi}_{2,0}$ (Å^3/μ_b^2)	$-2.2721 \cdot 10^{-1}$	$5.1668 \cdot 10^{-1}$	$-1.1556 \cdot 10^{-1}$	$8.0046 \cdot 10^{-2}$	$9.8746 \cdot 10^{-2}$
$\nu^{\Psi}_{4,0}$ (Å^3/μ_b^4)	$5.7501 \cdot 10^{-2}$	$-1.4534 \cdot 10^{-1}$	$1.7994 \cdot 10^{-2}$	$-1.1988 \cdot 10^{-2}$	$-3.1587 \cdot 10^{-2}$
$\nu^{\Psi}_{6,0}$ (Å^3/μ_b^6)	$-4.4203 \cdot 19^{-3}$	$1.7560 \cdot 10^{-2}$	$-9.0400 \cdot 10^{-4}$	$7.2805 \cdot 10^{-4}$	$3.4671 \cdot 10^{-3}$
$\kappa^{\Psi}_{2,0}$ (Å^3/μ_b^2)	$-1.1007 \cdot 10^{-1}$	$2.3675 \cdot 10^{-1}$	$6.0516 \cdot 10^{-3}$	$1.0087 \cdot 10^{-2}$	$-1.7967 \cdot 10^{-2}$
$\kappa^{\Psi}_{4,0}$ (Å^3/μ_b^4)	$2.7885 \cdot 10^{-2}$	$-1.0318 \cdot 10^{-1}$	$6.0184 \cdot 10^{-4}$	$-6.3490 \cdot 10^{-3}$	$6.3147 \cdot 10^{-3}$
$\kappa^{\Psi}_{6,0}$ (Å^3/μ_b^6)	$-1.7647 \cdot 10^{-3}$	$1.3267 \cdot 10^{-2}$	$-1.1180 \cdot 10^{-4}$	$9.1394 \cdot 10^{-4}$	$-5.0565 \cdot 10^{-4}$

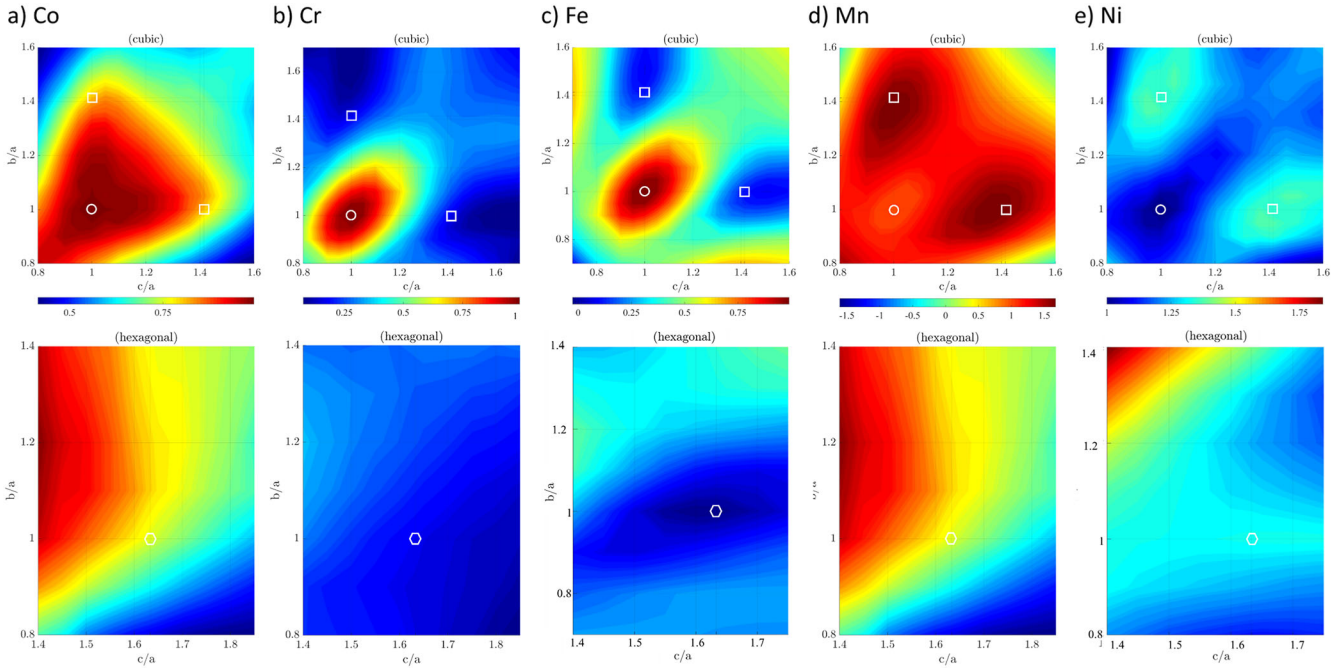

Fig. 7 | Distance dependent Ω_{nC} functions of the GUES. Ω_{nC} functions (Eq. (8)) describing the non-collinear magnetic contribution for **a** Co, **b** Cr, **c** Fe, **d** Mn and **e** Ni. Solid white dots indicate the $\Omega_{nC} = 1$ value, which correspond to BCC lattice, solid square dots FCC lattice, and solid hexagonal dots corresponds to perfect HPC lattice.

atoms. This is especially true for $\Phi_E(M)$ in Fe and Co atoms, which display negative values around 1.5–2.5 μ_b, while for Cr, Mn, and Ni, the increase of magnetic moment increases the Φ_E contribution to energy. That does not mean that Cr, Mn, and Ni do not display a ground state at magnetic configuration, but the responsibility of such ground state corresponds to other functions, Ψ_E, for the case of Ni (FM) and θ_E for Cr and Mn atoms, which display AFM ground state. This may be related to the type of electron itinerancy, more localized for Fe and Co due to the dominant influence of Φ_E, and very itinerant for Cr, Mn, and Ni where the Ψ_E and θ_E functions gain in importance[2]. The direct link to the theory of itinerant-electron magnetism from these results is not straightforward, and it is not the scope of this paper, but indeed, the results obtained have indeed some similarities.

It is there clear an increase of volume (see blue line in V_g functions in Fig. 9f–k) as the magnetic moment increases. Then, the FM and non-collinear contribution (in red and green color, respectively), which adds in general minor values of energy. This is the case, for instance, of Co and Ni, where this distribution of factors is more evident, as the blue line adds much more influence. The case of Fe is intermediate, where the ferromagnetic configuration may have a similar contribution as the Φ-functions. The Mn and Cr, which have the above-mentioned antiferromagnetic behavior, are clearly seen with the $\Omega_{nC} \cdot \Theta$ functions, which lower the energy and volume for such magnetic configuration.

In the subheading "Error analysis of the GUES", an error analysis can be seen in Fig. 2 for NM, FM, and AFM configurations using the fitted E_g, V_g, and K_g for each $\langle b/a, c/a, M\rangle$ combination for each element considered. It is important to note that each fitted energy in that figure uses the numerically fitted E_g, V_g, and K_g individually. This means that, for instance, the energy-volume relationship of the BCC lattice with $M = 0$ μ_b gives certain values of $\langle E_g, V_g, K_g\rangle$, and a FCC lattice at $M = 2$ μ_b provides at fitting other $\langle E_g, V_g, K_g\rangle$ values, independent of each other. The excellent fitting shown in Fig. 2 indeed showed that for any lattice and magnetic configuration, there are three values of $\langle E_g, V_g, K_g\rangle$ which predict the energy-volume relationship. The added value of the GUES is the description of inter-relationships between such (a priori independent) $\langle E_g, V_g, K_g\rangle$ parameters for different lattices and magnetic configurations. This has been explained in above, describing each contribution and the functional form of each of such

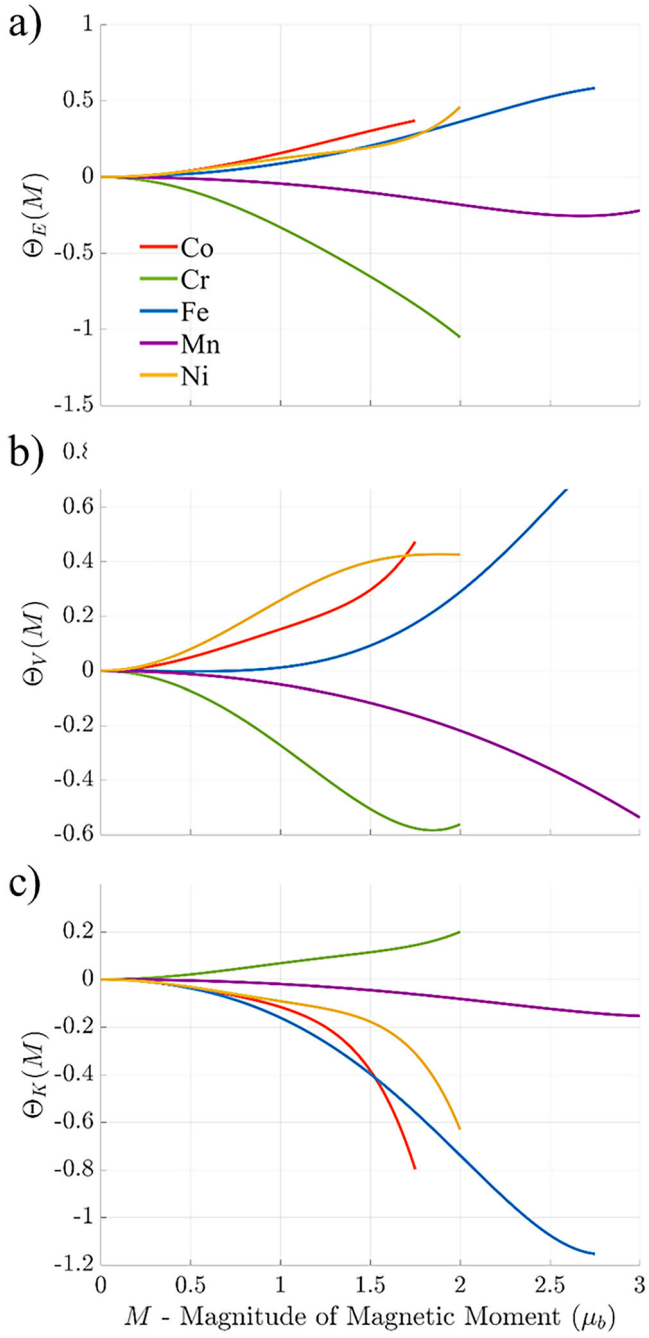

Fig. 8 | Magnetic dependent θ-functions of the GUES. Magnetic functions **a** θ_E, **b** θ_V and **c** θ_K for Co, Cr, Fe, Mn and Ni. Note that the legend is common for all figures and is indicated only in (**a**), and similarly, the x-axis is common for all figures but is only indicated in (**c**).

contributions, allowing to see the interrelationship between all $\langle E_g, V_g, K_g \rangle$ parameters at different lattices and magnetic configurations. Therefore, the prediction of the GUES by using Eq. (7) and the proposed Ω_0, Ω_M and Ω_{nC}, along with Φ-, Ψ-, and Θ-functions for each element, is different from the ones using directly the fitted $\langle E_g, V_g, K_g t \rangle$. The error in this case is logically larger (it cannot be better than the numerically fitted for each case), but provides a deep insight into the different factors contributing to the energy of the system and allows developing interatomic potentials, as the one in ref. 19, initially for ferromagnetic configuration, and now with the unified GUES proposed in this work, for non-collinear simulations, where a preliminary test is shown in the following subheading.

Figure 10 shows the comparison between the DFT calculated cohesive energy in the database corresponding to collinear DFT calculations and the GUES cohesive energy at predicting E_g, V_g, and K_g parameters by using the functions shown in Fig. 3 for Ω_0 (with the parameters of Table 1), Fig. 4 for Φ, Fig. 5 for Ω_M, Fig. 6 for Ψ, Fig. 7 for Ω_{nC}, and Fig. 8 for θ, with an RMSE of 3.8×10^{-4} eV. This RMSE is indeed higher than the one with the individually fitted E_g, V_g, and K_g parameters with a previously reported RMSE of 4.22×10^{-6} eV as shown in Fig. 2. The errors by different magnetic configurations are reasonably close to each other. In particular, the RMSE for non-magnetic is 6.23×10^{-4} eV, the RMSE for FM configuration is 4.05×10^{-4} eV, and the RMS for AFM is 2.59×10^{-4} eV. Although there are some differences at different magnetic configurations, the differences are small enough to be attributed to the numerical approach, rather than concluding that the GUES may have incorrect contributions due to different magnetic configurations. Also, the errors as a function of the magnitude of the magnetic moment does not follow any trend, being similar in value for all magnitudes of the magnetic moment, except for the highest values of AFM for Fe and Mn, which have an RMSE of 7.99×10^{-3} eV. As pointed out previously, the DFT calculations may have some convergence issues for configurations very far from equilibrium, which explains the increase in error. We conclude then that the predicted energies by the GUES show reasonably good results for all NM, FM, and AFM for cubic and hexagonal lattices and for all elements considered, considering especially the understanding that the GUES provides via the different contributions mentioned above.

Non-collinear calculations of the GUES

The proposed formulation for the GUES is intended in this work to unify the previously GUES formulation[19], which had different functions for FM and AFM configurations, making it impossible to transition between both configurations, nor perform non-collinear calculations. In this work, the Eq. (7) can be used to perform an initial check on the possibility of performing non-collinear calculations with the GUES, without the need of using Eq. (5), where the use of ω_0, ω_M, and ω_{nC} is formally needed. This is performed by keeping the lattice configuration fixed for the non-collinearity as explained in the subheading "Error analysis of the GUES", where different magnetic moment orientations are located in alternate (0,0,1) plane for cubic and (0,0,0,1) plane for hexagonal lattices, with the α_{ij} angle rotating between 0° and 180°. A similar lattice geometry with rotating magnetic moment in Fe for BCC (B2-like magnetic structures) was used in ref. 46, where a constrained density functional for non-collinear magnetism is proposed and in ref. 15 where a non-collinear magnetic atomic cluster expansion for iron is proposed.

As stated before, in this work, the distance-dependent functions ω_0, ω_M, and ω_{nC} are not determined here, since additional work must be performed in order to know their applicability for atomic coordinates outside ideal positions. Such ideal positions are understood in this case for all lattices considered, with fixed positions for all $\langle b/a, c/a \rangle$ cases for both cubic and hexagonal lattices. In our previous work, ω_0, ω_M were indeed successfully determined for Fe, where an extensive analysis was performed on transformation paths, vacancies, stresses, A15 and C15 lattices, elastic properties, dumbbell configurations, and γ-surfaces, demonstrating the existence of such functions and their predictability. With this in mind, the values of Ω_0, Ω_M, and Ω_{nC} are known since they were fitted for any lattice considered, and it is kept constant if rotations of magnetic moments are the only variable.

The non-collinear behavior in the case of Fe has special interest since a comparison can be performed with other approaches dealing with non-collinear simulations. The potential energy surface of the FM to AFM magnetic transformation, which is calculated as the ground state energy for spin rotation of the central atom in B2-like magnetic structure, i.e., alternating (0,0,1) planes, is displayed in Fig. 11a and the corresponding magnetic rotation energy barriers at constant magnetic moment is shown in Fig. 11b. Such energy barrier is seen to be quite dependent on the angle between magnetic moments, as well as on their magnitudes. The results are similar to those obtained in ref. 15. A relationship between the ground state energy and corresponding magnetic moment for BCC can also be calculated

Table 4 | Values of the ε, ν, κ parameters for θ functions for Co, Cr, Fe, Mn and Ni

Parameter (units	Co	Cr	Fe	Mn	Ni
$\varepsilon^{\theta}_{2,0}$ (eV/μ_b^2)	$1.7746 \cdot 10^{-1}$	$-4.3157 \cdot 10^{-1}$	$1.0062 \cdot 10^{-1}$	$-3.9894 \cdot 10^{-2}$	$1.8388 \cdot 10^{-1}$
$\varepsilon^{\theta}_{4,0}$ (eV/μ_b^4)	$-2.0576 \cdot 10^{-2}$	$6.0322 \cdot 10^{-2}$	$2.8541 \cdot 10^{-3}$	$-3.7965 \cdot 10^{-3}$	$-7.6768 \cdot 10^{-2}$
$\varepsilon^{\theta}_{6,0}$(eV/$\mu_b^6$)	$7.0767 \cdot 10^{-4}$	$-3.3319 \cdot 10^{-3}$	$-7.8403 \cdot 10^{-4}$	$6.1270 \cdot 10^{-4}$	$1.4894 \cdot 10^{-2}$
$\nu^{\theta}_{2,0}$ (Å^3/μ_b^2)	$1.0893 \cdot 10^{-1}$	$-3.0320 \cdot 10^{-2}$	$-5.7402 \cdot 10^{-2}$	$-2.4103 \cdot 10^{-2}$	$1.7092 \cdot 10^{-1}$
$\nu^{\theta}_{4,0}$ (Å^3/μ_b^4)	$-4.3423 \cdot 10^{-2}$	$-6.1457 \cdot 10^{-2}$	$3.1727 \cdot 10^{-2}$	$-9.6617 \cdot 10^{-4}$	$-4.5446 \cdot 10^{-2}$
$\nu^{\theta}_{6,0}$ (Å^3/μ_b^6)	$1.0806 \cdot 10^{-2}$	$8.6899 \cdot 10^{-3}$	$-2.5282 \cdot 10^{-3}$	$3.5872 \cdot 10^{-5}$	$4.0124 \cdot 10^{-3}$
$\kappa^{\theta}_{2,0}$ (Å^3/μ_b^2)	$6.7681 \cdot 10^{-2}$	$4.9001 \cdot 10^{-2}$	$-7.8558 \cdot 10^{-2}$	$-1.4016 \cdot 10^{-2}$	$-7.1282 \cdot 10^{-2}$
$\kappa^{\theta}_{4,0}$ (Å^3/μ_b^4)	$-6.8881 \cdot 10^{-2}$	$-1.3026 \cdot 10^{-2}$	$-2.3531 \cdot 10^{-3}$	$4.3749 \cdot 10^{-3}$	$3.4764 \cdot 10^{-2}$
$\kappa^{\theta}_{6,0}$ (Å^3/μ_b^6)	$1.3164 \cdot 10^{-2}$	$1.5704 \cdot 10^{-3}$	$5.7457 \cdot 10^{-4}$	$-5.6377 \cdot 10^{-4}$	$-9.1676 \cdot 10^{-3}$

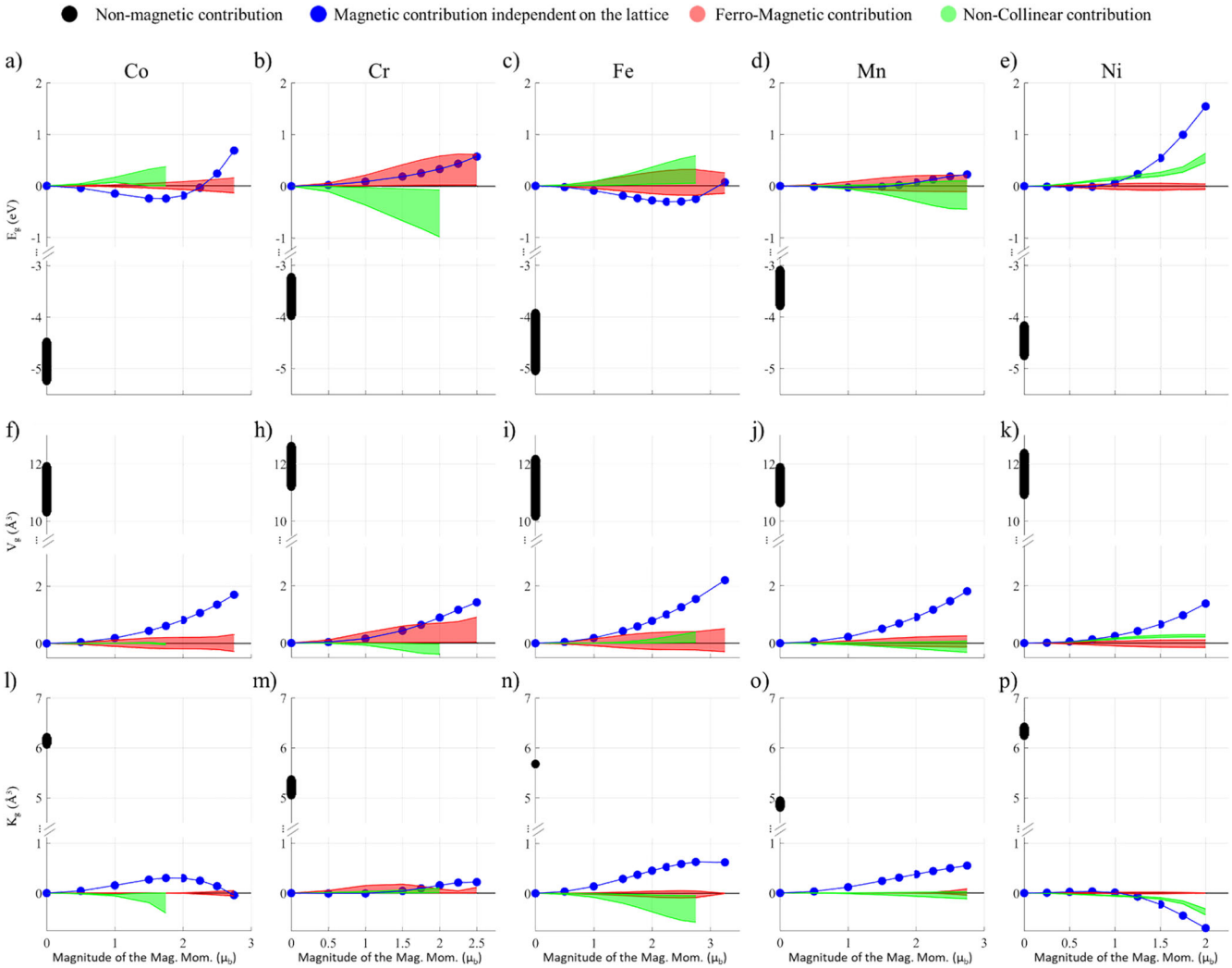

Fig. 9 | Contribution of each function to the GUES. Contribution of the non-magnetic functions, magnetic, ferromagnetic and non-collinear into E_g, V_g, and K_g for Co (**a**, **f**, **l**), Cr (**b**, **h**, **m**), Fe (**c**, **i**, **n**), Mn (**d**, **j**, **o**) and Ni (**e**, **k**, **p**) respectively. Note that the legend is common for all figures and is indicated only at the top of the figure. The *x*-axis is common for all figures but isonly indicated in the bottom images, and similarly the *y*-axis is indicated only in (**a**, **f**, **l**).

for the ground state cell parameter, and analyze the variation of the magnetic behavior from FM to AFM, as depicted in Fig. 11c. The ground state energy increases from FM to AFM, while the magnetic moment accordingly. The results are consistent with the results shown in ref. 46.

In order to fully analyse the behavior of non-collinear calculations in all elements considered in this work, a set of non-collinear simulations concerning Co, Cr, Fe, Mn, and Ni have performed DFT calculations with B2-likd lattices for BCC Cr and Fe, $L1_0$-like magnetic configuration for FCC Mn and Ni, and be a B_h-like magnetic configuration for HCP Co. The same AFM configuration described in the Methods heading is also applied here where the spins rotate in different angles (30°, 45°, 90°, 120° 135° and 150°) in alternate (0,0,1) planes for the cubic-based lattices and (0,0,0,1) base plane

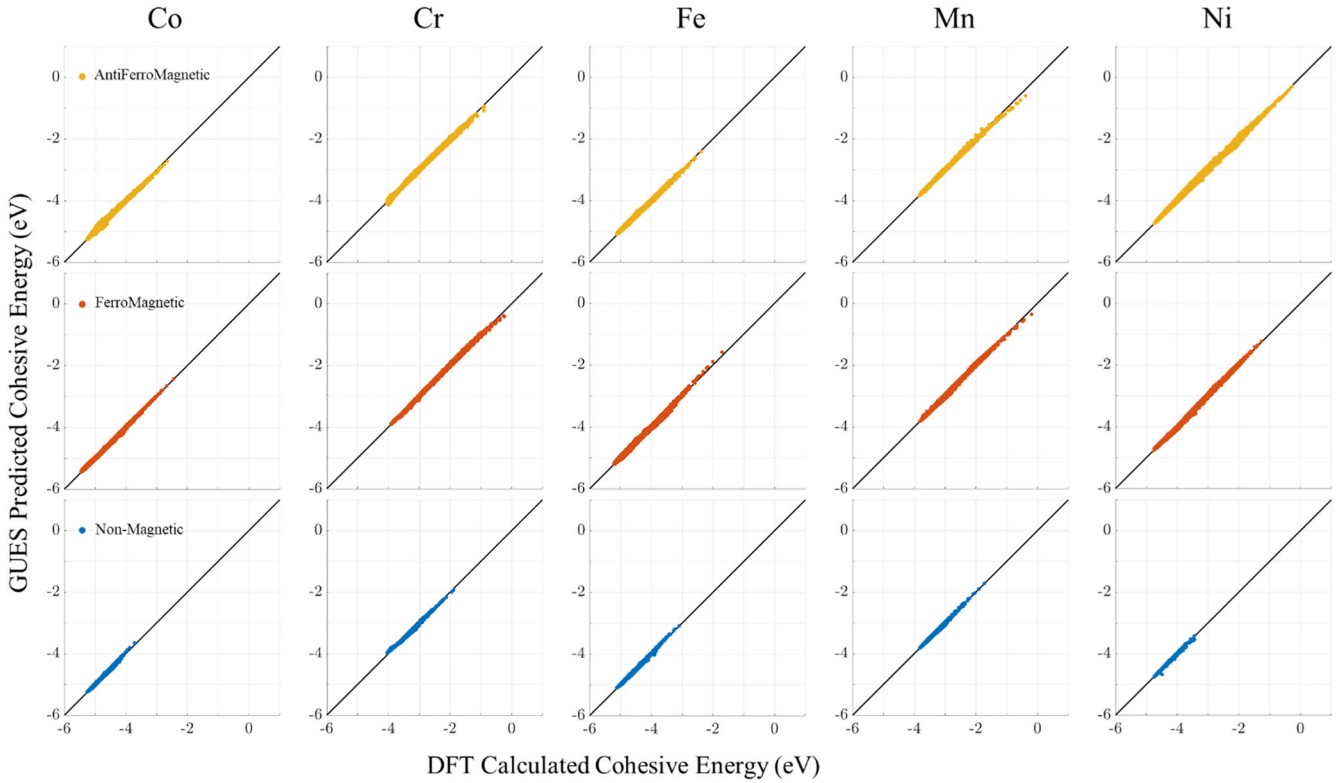

Fig. 10 | GUES predictions of the energy by using the fitted functions. DFT calculated cohesive energy vs. GUES predicted cohesive energy with predicted E_g, V_g, and K_g, for Co, Cr, Fe, Mn, and Ni, in non-magnetic, ferromagnetic, and antiferromagnetic for all cubic- and hexagonal-based lattices. The RMSE = 3.8×10^{-4} eV corresponds to all data considered.

for the hexagonal-based lattices, keeping the same magnitude of the magnetic moments in the cell. Note that the angles 0° and 180° correspond to pure FM and AFM, respectively, and are already considered in the Results heading.

The DFT *vs.* GUES calculations are shown in Fig. 12, where a reasonably good fit is observed at varying the misorientation angles. The colors correspond to different angles, where in this figure, the magnitude of the magnetic moment is not explicitly indicated, but they actually vary from 0.4 μ_b to 2.7 μ_b approximately. The lattices and the type of rotation are indicated in each image. The comparison of the DFT vs. GUES includes the complete database created for the GUES fitting (depicted with black dots), in order to visualize the performance of the GUES in non-collinear calculations as compared to the complete GUES predictive capability.

There are indeed some differences between the DFT and GUES calculations, but the trends at varying the angle and magnitude of the magnetic moments are indeed correct and display an error of similar magnitude to the one for pure FM and AFM calculations. This is especially relevant in this work since this is the first data that is not used for the Ω-, Φ-, Ψ-, and Θ-functions fitting, and they represent the first check that the formulation proposed, so far, captures the non-collinear behavior, which needs to be confirmed in future steps for other lattices and mixtures of magnetic moments. More precisely, the RMSE of each case between the DFT and GUES in the non-collinear calculations is $5.9 \cdot 10^{-3}$ eV for Co, $3.7 \cdot 10^{-2}$ eV for Cr, $1.1 \cdot 10^{-3}$ eV for Fe, $8.6 \cdot 10^{-3}$ eV for Mn, and $6.0 \cdot 10^{-3}$ eV for Ni. The errors are indeed one order of magnitude larger than the RMSE predicted for the whole database reported previously of $3.8 \cdot 10^{-4}$ eV in the previous subheading "Factor Analysis and predictability of the GUES" for the NM, FM, and AFM cases. This comes from the fact that the non-collinear DFT calculations are not included in the development of the Ω_0, Ω_M, Ω_{nC}, and Φ-, Ψ-, and Θ-functions, but still the approach shows good predictability and transferability between the initial FM and AFM cases to non-collinear case. Additionally, the case of Cr shows a larger error compared to other elements. An analysis on the errors of the fitted GUES (FM and AFM data) for Cr around BCC shows larger errors as compared to other structures, which explains such larger difference, and further investigation is required in this element.

It is clear that further research is needed to improve the non-collinear calculations, either considering additional exponents of M in the Φ-, Ψ-, and Θ-functions (up to M^8, M^{10}, or further) or in the angle dependence of the Θ-functions, which controls the non-collinearity contribution, adding for instance up to $\left(\sin\left(\frac{\alpha}{2}\right)\right)^4$ or further terms.

Discussion

This work represents a qualitative improvement of the initial proposed GUES in ref. 19, where a new magnetic interatomic potential was presented, based on a generalization of the universal equation of states able to predict the magnetic-dependent energy of the magnetic 3 d transition elements. Such a magnetic interatomic potential was developed only for FM configurations, while the initial formulation did not allow for other forms of magnetism. Specifically, the AFM configuration, also included in the GUES, was not described in the magnetic interatomic potential developed for FM. In this work, the GUES has been modified in a way that both FM and AFM can be described under the same formulation. This is actually done by including the non-collinear configuration by adding the angles between different magnetic moments, which indeed includes the AFM and any other magnetic configuration. With this, a paramount improvement has been possible, since now the formulation allows for ferromagnetic, ferrimagnetic, antiferromagnetic, paramagnetic, or any non-collinear magnetic configuration. Additionally, the GUES was postulated only for Fe, where additional work for other elements had to be performed to guarantee the applicability of this approach to other elements.

Therefore, two main advances have been carried out in this work. Firstly, the application of the GUES with other elements, namely the rest of the magnetic 3 d transition metals Co, Cr, Mn, and Ni for cubic and hexagonal lattices, in addition to the extension of the case of Fe for hexagonal

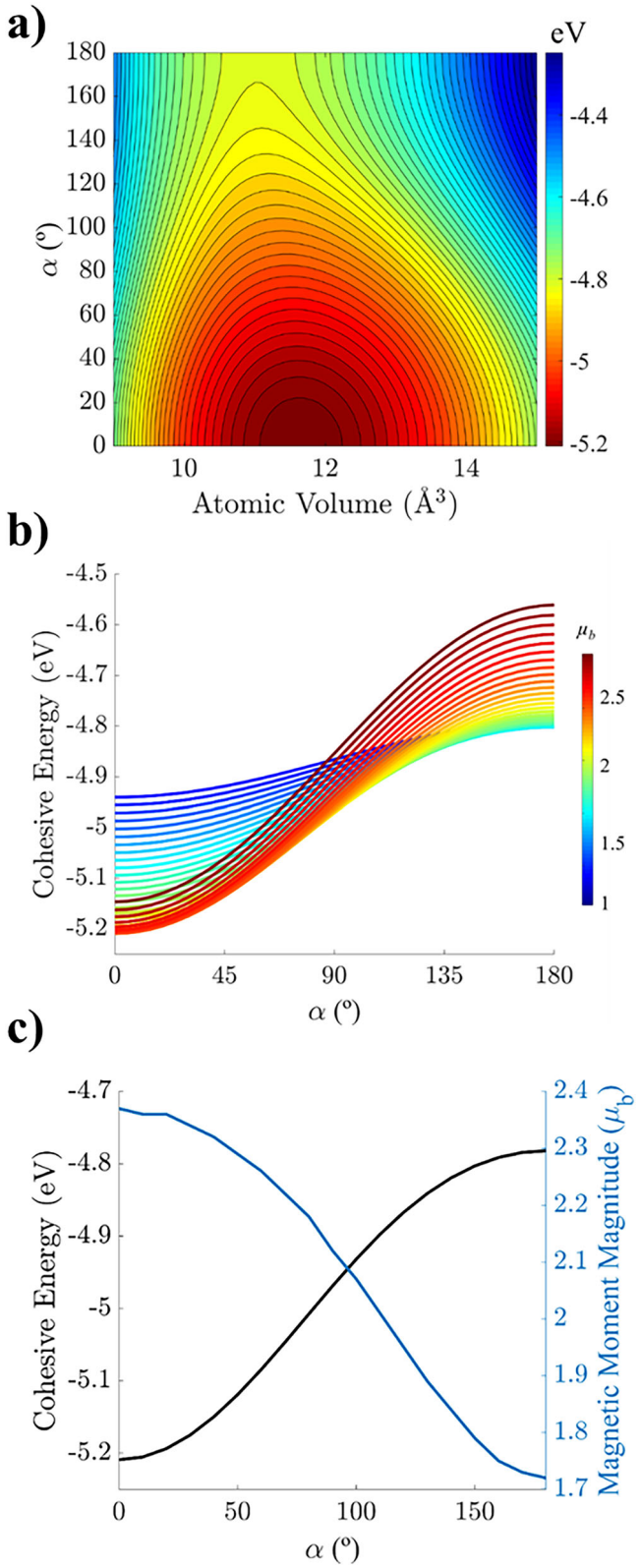

Fig. 11 | Non-collinear calculations for Fe, energy barriers, and ground states. **a** Contourplot of the FM to AFM spin rotation with alternate (0,0,1) planes in B2-like magnetic structure, **b** FM to AFM magnetic rotation energy barriers at constant magnetic moment with alternate (0,0,1) planes in B2-like magnetic structure. In both figures, α indicates the spin rotation angle from FM (0°) to AFM (180°), **c** Ground state energy and corresponding magnitude of the magnetic moments for FM to AFM transformation in B2-like magnetic structure with ell parameter 2.8561 Å.

lattices, which was not included initially. The results indicate that the GUES indeed describes the energy of such elements, while the approach is consistent within the Stoner model of band magnetism, the Ginzburg-Landau approximation used in the magnetic cluster expansion method, as well as the non-collinear magnetism within the Heisenberg-Landau Hamiltonians. Although the GUES is not confirmed to other elements, the results suggest that it can be applicable to other elements, especially metals, which share similar characteristics with Co, Cr, Fe, Mn, and Ni. Secondly, the unification of all magnetic configurations in one formulation is demonstrated for FM and AFM in all cases: a large variety of cubic and hexagonal (with all possible deformations), and for all elements considered here. A preliminary exploration of the possibility of predicting non-collinear simulations has been performed for all elements. In order to carry out this, some restrictions are imposed on the magnitude of the magnetic moments considered (with different angles between them), which allowed to use the GUES using the Ω_0, Ω_M, and Ω_{nC} functions, without the need to develop formally the interatomic potential. This must be done in order to run non-collinear simulations and needs the description of the ω_0, ω_M, and ω_{nC} distance-dependent functions, which provide Ω_0, Ω_M, and Ω_{nC} when they are evaluated for the set of distances of each lattice.

Additional work must be performed in order to confirm the possibility of running non-collinear simulations at finite temperature, which is the ultimate goal of this potential, but the preliminary results are very motivating and encourage to continue analysing this formulation as an alternative to other formulations where the non-collinear simulations are still elusive.

Methods

DFT calculations and database

In order to analyse the existence of functions for the proposed unified formulation, a non-collinear term has been introduced, describing therefore both FM and AFM configurations, in both cubic and hexagonal lattices. The existence of such functions for Co, Cr, Mn, and Ni has been demonstrated before, proving the robustness of the proposed formulation. Here, a description of the database employed is presented.

A large database of DFT calculations on Cr, Co, Fe, Mn and Ni systems has been performed using Vienna Ab initio Simulation escribes the large DFT database employed on Cr, Co, Fe, Mn and Ni systems has been performed using Vienna Ab initio Simulation Package (VASP)[47,48] using the projector augmented-wave (PAW) method[49] and the Perdew-Burke-Ernzerhof generalized gradient functional[50] with collinear spin polarization. The core configuration for the PAW potentials used in this paper was $[Ar]3d^84s^1$ for Co, $[Ar]3d^54s^1$ for Cr, $[Ar]3d^74s^1$ for Fe, $[Ar]3d^64s^1$ for Mn, and $[Ar]3d^94s^1$ for Ni. The calculations utilized a plane-wave cutoff energy of 400 eV. Total energies were computed using a Γ-centered Monkhorst-Pack mesh[51] of k-points with a spacing of 0.16 $Å^{-1}$, corresponding to a $14 \times 14 \times 14$ k-point grid for a two-atom BCC unit cell with a lattice parameter of 2.831 Å. Therefore, these calculations were performed similarly as the ones in ref. 19 where additional calculations with larger k-mesh (mesh spacing of 0.16 $Å^{-1}$) were performed to check the accuracy for Fe. It is assumed that good accuracy is reached in this work also for Co, Cr, Mn, and Ni. In this regard, the computational parameters were selected based on convergence tests performed for Fe in our previous study[19], where a finer k-mesh was tested to ensure sufficient accuracy. To maintain consistency and allow direct comparison, the same settings were applied to Co, Cr, Mn, and Ni. Given the similar electronic and magnetic properties of these transition metals, the chosen parameters are expected to provide a comparable level of accuracy. Furthermore, a detailed convergence study using similar computational parameters was conducted in our previous work on high-entropy alloys from the Fe-Cr-Mn-Ni system[52] which includes the same elements studied here. Since these settings provided reliable results for complex multicomponent systems, they can be considered well-suited for the pure elements investigated in this study.

In order to know the energies of cubic-based structures, rectangular cuboids corresponding to the relative positions (0,0,0) and (0.5,0.5,0.5) of

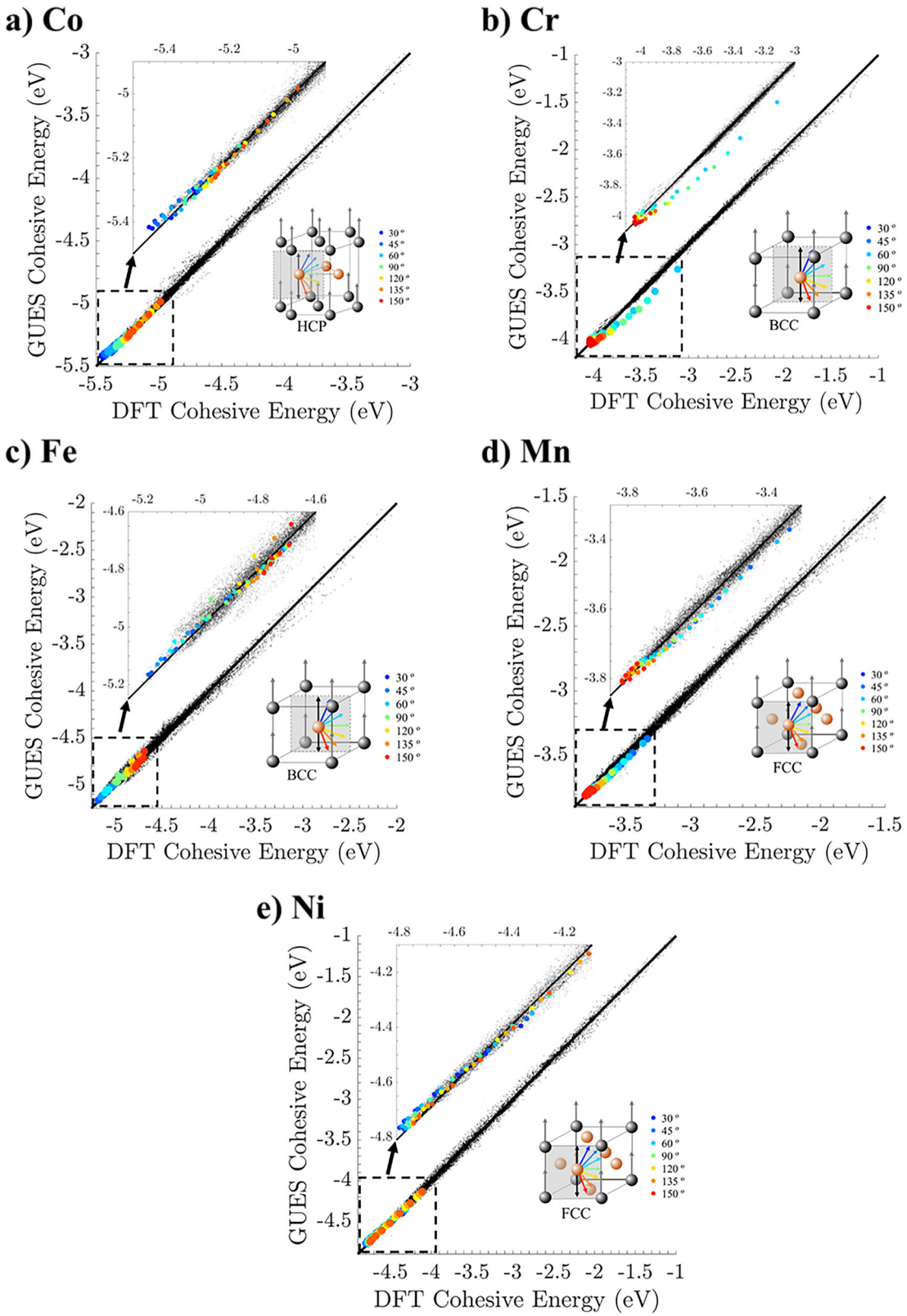

Fig. 12 | Non-collinear calculations for Co, Cr, Fe, Mn and Ni. Comparison between the DFT and GUES cohesive energies for the non-collinear configurations where the colours indicate the rotation angle as shown in the legend. The rotation plane is indicated in each image. The complete set of non-magnetic, ferromagnetic and antiferromagnetic DFT vs predicted GUES cohesive energies are also displayed in black dots for comparison purposes, and correspond to the same comparison of Fig. 11. **a** Co HCP lattice, **b** Cr BCC lattice, **c** Fe BCC lattice, **d** Mn FCC Lattice and **e** Ni FCC lattice.

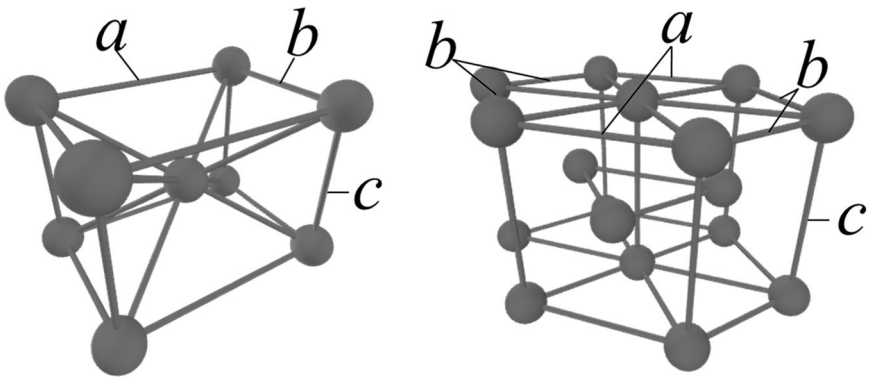

Fig. 13 | Illustration of the lattices employed for the DFT calculations. Illustration of the cubic-based (left) and hexagonal-based (right) structures and their respective cell parameters.

the cubic cell, and different *b/a* and *c/a* ratios, being *a*, *b*, and *c* are the three lattice magnitudes of the corresponding body-centered orthorhombic structure as seen in Fig. 13 (left-hand side). Similarly, for the hexagonal-based structures, the relative positions (1/3,2/3,1/4) and (2/3,1/3,3/4) of the considered hexagonal cell, and different *b/a* and *c/a* ratios, being *a*, *b*, and *c* are the three lattice magnitudes of the corresponding hexagonal close-packed structure as seen in Fig. 13 (right-hand side). Note that *a*, *b*, and *c* will correspond to lattice parameters of both cubic and hexagonal lattices, and they will be referred accordingly.

The database then contains all combinations where *c/a* and *b/a* vary independently, taking the values 0.7, 0.8, 0.9, 0.95, 1, 1.05, 1.1, 1.2, 1.3, 1.35, $\sqrt{2}$, 1.45, 1.5, 1.6 and 1.7 in the cubic case, while on the hexagonal case *b/a* can take the values 0.6, 0.7, 0.8, 0.9, 1, 1.1, 1.2, 1.3 and 1.4 and c/a takes 1.4, 1.45, 1.5, 1.55, 1.6, $\sqrt{8/3}$, 1.65, 1.7, 1.75, 1.8 and 1.85. In the case of the hexagonal deformations, all possible $\langle b/a, c/a\rangle$ combinations are considered, but for the case of cubic deformations, due to the symmetry, only half of them are considered (for instance, $\langle b/a = 0.9, c/a = 1.45\rangle$ is the same lattice as $\langle b/a = 1.45, c/a = 0.9\rangle$). Note that, in the cubic-based structures $\langle b/a = 1, c/a = 1t\rangle$ corresponds to pure BCC, while $\langle b/a = 1, c/a = \sqrt{2}\rangle$ is the FCC structure. Also, a perfect HCP is while $\left\langle b/a = 1, c/a = \sqrt{8/3}\right\rangle$ for the hexagonal-based structures. With this, the number of different cubic lattices is 120, while the number of different hexagonal lattices is 99. There is indeed a large variability of lattices and interatomic distances covering ground states as well as structures very far from ground state or the most common structures.

In addition to this, each of these 219 different lattices is calculated in 8 different volumes, namely 9.25 Å^3, 9.75 Å^3, 10.25 Å^3, 10.75 Å^3, 11.25 Å^3, 11.75 Å^3, 12.25 Å^3, and 11.75 Å^3, covering in general all ground states for the considered elements and crystal lattices. This represents 1752 different altogether atomic configurations. Again, every of this 1752 atomic configurations is calculated in NM (with $M = 0\,\mu_b$), FM configuration at $M = 0.5\,\mu_b$, $1\,\mu_b$, $1.5\,\mu_b$, $1.75\,\mu_b$, $2\,\mu_b$, $2.25\,\mu_b$, $2.5\,\mu_b$, $2.75\,\mu_b$, $3.25\,\mu_b$, and AFM configuration (constrained magnetic calculations) with 9 magnitudes of the magnetic moment spacing between $0.5\,\mu_b$ and $3.5\,\mu_b$. The AFM configuration will be $\langle\uparrow(0,0,0),\downarrow(\frac{1}{2},\frac{1}{2},\frac{1}{2})\rangle$ of the cubic cell, where the arrows indicate the spin orientation, and the numbers are the relative positions of the rectangular cuboids. For the hexagonal-based structures, the AFM configuration will be $\langle\uparrow(\frac{1}{3},\frac{2}{3},\frac{1}{4}),\downarrow(\frac{2}{3},\frac{1}{3},\frac{3}{4})\rangle$. With this, the structures alternate spin-up—spin-down layers in the (0,0,1) plane for the cubic-based lattices and (0,0,0,1) base plane for the hexagonal-based lattices. Therefore, the BCC AFM would be a B2-like magnetic configuration, the FCC would be a $L1_0$-like magnetic configuration, and the HCP would be a B_h-like magnetic configuration.

In the AFM case, the magnitudes of the magnetic moments are not strictly fixed due to the way VASP handles constrained calculations; however, the variation of energy as a function of magnetic moment is well captured. To assess the effect of constraint strength, different penalty parameters (denoted λ parameter in ref. 46) were tested, and while variations in total energy and magnetic moments were observed, the corrected energy (total energy minus penalty energy) as function of λ between 1 and 5 eV/μ_b^2 remained a reliable measure of the system's energy relative to its magnetic moment in all cases. Therefore, in all constrained calculations, the penalty parameter was set to 1 eV/μ_b^2. With this 33288 DFT calculations, varying structure, volume, magnetic configuration, and magnetic moment for each element have been performed, representing 166440 DFT calculations. Some of the calculations have convergence difficulties for combinations of $\langle b/a, c/a, V, M\rangle$ very far from the ground state (especially in the case of AFM configuration). Therefore, some of them are discarded, and replaced with others closer to equilibrium, especially in the case of Ni, whose cohesive energy increase very rapidly with increasing magnetic moment.

Data availability

The D.F.T. dataset used for the GUES fitting can be available from the corresponding author on reasonable request

Received: 5 December 2024; Accepted: 26 August 2025;
Published online: 10 October 2025

References

1. Hasegawa, H. & Pettifor, D. G. Microscopic theory of the temperature-pressure phase diagram of iron. *Phys. Rev. Lett.* **50**, 130–133 (1983).
2. Kübler, J. *Theory of Itinerant Electron Magnetism* (Oxford Univerity Press, 2021).
3. Nguyen-Manh, D. & Dudarev, S. L. Model many-body Stoner Hamiltonian for binary FeCr alloys. *Phys. Rev. B - Condens. Matter Mater. Phys.* **80**, 1–11 (2009).
4. Drautz, R. & Fähnle, M. Spin-cluster expansion: parametrization of the general adiabatic magnetic energy surface with ab initio accuracy. *Phys. Rev. B* **69**, 104404 (2004).
5. Drautz, R. & Fähnle, M. Parametrization of the magnetic energy at the atomic level. *Phys. Rev. B* **72**, 212405 (2005).
6. Lavrentiev, M. Y., Nguyen-Manh, D. & Dudarev, S. L. Magnetic cluster expansion model for bcc-fcc transitions in Fe and Fe-Cr alloys. *Phys. Rev. B* **81**, 1–6 (2010).
7. Nguyen-Manh, D., Ma, P. W., Lavrentiev, M. Y. & Dudarev, S. L. Constrained non-collinear magnetism in disordered Fe and Fe-Cr alloys. *Ann. Nucl. Energy* **77**, 246–251 (2015).
8. Ma, P. W., Dudarev, S. L. & Wróbel, J. S. Dynamic simulation of structural phase transitions in magnetic iron. *Phys. Rev. B* **96**, 1–17 (2017).
9. Ruban, A. V., Khmelevskyi, S., Mohn, P. & Johansson, B. Temperature-induced longitudinal spin fluctuations in Fe and Ni. *Phys. Rev. B* **75**, 054402 (2007).
10. Ma, P. & Dudarev, S. L. Longitudinal magnetic fluctuations in Langevin spin dynamics. *Phys. Rev. B* **86**, 054416 (2012).
11. Lavrentiev, M. Y., Wróbel, J. S., Nguyen-Manh, D. & Dudarev, S. L. Magnetic and thermodynamic properties of face-centered cubic Fe-Ni alloys. *Phys. Chem. Chem. Phys.* **16**, 16049 (2014).

12. Nikolov, S. et al. Data-driven magneto-elastic predictions with scalable classical spin-lattice dynamics. *npj Comput Mater* **7**, 1–12 (2021).
13. Novikov, I., Grabowski, B., Kormann, F. & Shapeev, A. Magnetic Moment Tensor Potentials for collinear spin-polarized materials reproduce different magnetic states of bcc Fe. *npj Comput Mater* **8**, 13 (2022).
14. Chapman, J. B. J. & Ma, P. W. A machine-learned spin-lattice potential for dynamic simulations of defective magnetic iron. *Sci. Rep.* **12**, 1–15 (2022).
15. Rinaldi, M., Mrovec, M., Bochkarev, A., Lysogorskiy, Y. & Drautz, R. Non-collinear magnetic atomic cluster expansion for iron. *npj Comput Mater* **10**, 1–12 (2024).
16. Eckhoff, M. & Behler, J. High-dimensional neural network potentials for magnetic systems using spin-dependent atom-centered symmetry functions. *npj Comput Mater* **7**, 1–11 (2021).
17. Li, H. et al. Deep-learning electronic-structure calculation of magnetic superstructures. *Nat. Comput. Sci.* **3**, 321–327 (2023).
18. Khatri, Y. & Kashyap, A. Advancing magnetic material discovery through machine learning: unveiling new manganese-based materials. *APL Mach. Learn.* **1**, 046113 (2023).
19. Toda-caraballo, I., Wr¢bel, J. S. & Nguyen-Manh, D. Generalized universal equation of states for magnetic materials: a novel formulation for an interatomic potential in Fe. *Phys. Rev. Mater* **6**, 043806 (2022).
20. Rose, J. H., Smith, J. R., Guinea, F. & Ferrante, J. Universal features of the equation of state of metals. *Phys. Rev. B* **29**, 2963–2969 (1984).
21. Vinet, P., Rose, J. H., Ferrante, J. & Smith, J. R. Universal features of the equation of state of solids. *J. Phys. Condens. Matter* **1**, 1941–1963 (1989).
22. Daw, M. S. & Baskes, M. I. Semiempirical, quantum mechanical calculation of hydrogen embrittlement in metals. *Phys. Rev. Lett.* **50**, 1285–1288 (1983).
23. Daw, M. S. & Baskes, M. I. Embedded-atom method: derivation and application to impurities, surfaces, and other defects in metals. *Phys. Rev. B* **29**, 6443–6453 (1984).
24. Dudarev, S. L. & Derlet, P. M. A. 'magnetic' interatomic potential for molecular dynamics simulations. *J. Phys. Condens. Matter* **17**, 7097–7118 (2005).
25. Derlet, P. M. & Dudarev, S. L. Million-atom molecular dynamics simulations of magnetic iron. *Prog. Mater. Sci.* **52**, 299–318 (2007).
26. Ercolessi, F. & Tosatti, E. Au (100) surface reconstruction. *Phys. Rev. Lett.* **57**, 719–722 (1986).
27. Ercolessi, F., Parrinello, M. & Tosatti, E. Simulation of gold in the glue model. *Philos. Mag. A* **58**, 213–226 (1988).
28. Shapeev, A. V. Moment tensor potentials: a Class of systematcially improvable interatomic potentials. *Soc. Ind. Appl. Math.* **14**, 1153–1173 (2016).
29. Jelinek, B. et al. Modified embedded atom method potential for Al, Si, Mg, Cu, and Fe alloys. *Phys. Rev. B* **85**, 245102 (2012).
30. Ravindran, P. et al. Density functional theory for calculation of elastic properties of orthorhombic crystals: Application to TiSi2. *J. Appl. Phys.* **84**, 4891–4904 (1998).
31. Togo, A. & Tanaka, I. First principles phonon calculations in materials science. *Scr. Mater.* **108**, 1–5 (2015).
32. Fujihisa, H. & Takemura, K. Stability and the equation of state of alpha-manganese under ultrahigh pressure. *Phys. Rev. B* **52**, 13257–13260 (1995).
33. Sha, X. & Cohen, R. E. First-principles thermal equation of state and thermoelasticity of hcp Fe at high pressures. *Phys. Rev. B* **81**, 1–33 (2010).
34. Mishin, Y., Mehl, M., Papaconstantopoulos, D., Voter, A. & Kress, J. Structural stability and lattice defects in copper: Ab initio, tight-binding, and embedded-atom calculations. *Phys. Rev. B* **63**, 1–16 (2001).
35. Roy, P. B. & Roy, S. B. Applicability of three-parameter equation of state of solids: Compatibility with first principles approaches and application to solids. *J. Phys. Condens. Matter* **15**, 1643–1663 (2003).
36. Baskes, M. I. Application of the embedded-atom method to covalent materials: a semiempirical potential for silicon. *Phys. Rev. Lett.* **59**, 2666–2669 (1987).
37. Baskes, M. I., Nelson, J. S. & Wright, A. F. Semiempirical modified embedded-atom potentials for silicon and germanium. *Phys. Rev. B* **40**, 6085–6100 (1989).
38. Baskes, M. I. Modified embedded-atom potentials for cubic materials and impurities. *Phys. Rev. B* **46**, 2727–2742 (1992).
39. Landau, L. D., Lifshitz, E. M. Statistical Physics (Pergamon Press, 1976).
40. Finnis, M. W. & Sinclair, J. E. A simple empirical N-body potential for transition metals. *Philos. Mag. A* **50**, 45–55 (1984).
41. Lin, Y. S., Mrovec, M. & Vitek, V. Bond-order potential for magnetic body-centered-cubic iron and its transferability. *Phys. Rev. B* **93**, 1–11 (2016).
42. Lizárraga, R. et al. First principles theory of the hcp-fcc phase transition in cobalt. *Sci. Rep.* **7**, 6–13 (2017).
43. Liu, G., Nguyen-Manh, D., Liu, B. G. & Pettifor, D. G. Magnetic properties of point defects in iron within the tight-binding-bond Stoner model. *Phys. Rev. B* **71**, 1–8 (2005).
44. Lu, Z., Zhu, W., Lu, T. & Wang, W. Does the fcc phase exist in the Fe bcc-hcp transition? A conclusion from first-principles studies. *Model. Simul. Mater. Sci. Eng.* **22**, 025007 (2014).
45. Müller, M., Erhart, P. & Albe, K. Analytic bond-order potential for bcc and fcc iron - Comparison with established embedded-atom method potentials. *J. Phys. Condens. Matter* **19**, 326220 (2007).
46. Ma, P. W. & Dudarev, S. L. Constrained density functional for noncollinear magnetism. *Phys. Rev. B* **91**, 054420 (2015).
47. Kresse, G. & Furthmüller, J. Efficiency of ab-initio total energy calculations for metals and semiconductors using a plane-wave basis set. *Comput. Mater. Sci.* **6**, 15–50 (1996).
48. Kresse, G. & Furthmüller, J. Efficient iterative schemes for ab initio total-energy calculations using a plane-wave basis set. *Phys. Rev. B* **54**, 11169–11186 (1996).
49. Blöchl, P. E. Projector augmented-wave method. *Phys. Rev. B* **50**, 17953–17979 (1994).
50. Perdew, J. P., Burke, K. & Ernzerhof, M. Generalized gradient approximation made simple. *Phys. Rev. Lett.* **77**, 3865–3868 (1996).
51. Monkhorst, H. J. & Pack, J. D. Special points for Brillouin-zone integrations. *Phys. Rev. B* **13**, 5188–5192 (1976).
52. Fedorov, M., Wróbel, J. S., Fernández-Caballero, A., Kurzydłowski, K. J. & Nguyen-Manh, D. Phase stability and magnetic properties in fcc Fe-Cr-Mn-Ni alloys from first-principles modeling. *Phys. Rev. B* **101**, 1–30 (2020).

Acknowledgements

The authors are grateful for financial support of the project INNUMAT (Ref: 101061241), from the Euratom Program HORIZON-EURATOM-2021-NRT-01. The simulations were carried out with the support of the Interdisciplinary Centre for Mathematical and Computational Modeling (ICM), University of Warsaw, under grant No. GB79-6. ITC would like to thank to the DIGImeTAL project (Ref: TED2021-132214B-I00), from the Proyectos Estratégicos Orientados a la Transición Ecológica y a la Transición Digital 2021, funded by the Plan de Recuperación, Transformación y Resiliencia, Spanish Ministerio de Ciencia, Innovación y Universidades. This work has also been carried out within the framework of the EUROfusion Consortium, from which JSW and DNM have received funding from the Euratom research and training program 2014-2018 and 2019-2020 under grant agreement No 633053. The views and opinions expressed herein do not necessarily reflect those of the European Commission. DNM's work is supported by the UK-EPSRC Energy Program [grant number EP/W006839/1]. Finally, JSW and DNM acknowledge the support from high-performing computing facility MARCONI (Bologna, Italy) provided by EUROfusion. The authors are also grateful to the Digital Laboratory of Metallurgy from CENIM-CSIC and the access to the high-performing server facilities.

Author contributions

The methodology was proposed by I.T.C., and all authors contribute to the concept of the work. The D.F.T. database was developped by J.S.W. and I.T.C., and the D.F.T. calculations were made by J.S.W. and suppervised by D.N.M. Data I.T.C. wrote the main manuscript text and prepared the figures and tables, and J.S.W. and D.N.M. reviewed the manuscript.

Competing interests

The authors declare no competing interests.

Additional information

Supplementary information The online version contains supplementary material available at https://doi.org/10.1038/s41524-025-01783-3.

Correspondence and requests for materials should be addressed to Isaac Toda-Caraballo.